Aus der

Neurologischen Klinik und Poliklinik

Klinikum der Ludwig-Maximilians-Universität München

und dem

Deutschen Zentrum für Neurodegenerative Erkrankungen (DZNE)

The Role of Insulin-Degrading Enzyme in Regulating α-Synuclein Aggregation and Toxicity

Dissertation

zum Erwerb des Doktorgrades der Medizin

an der Medizinischen Fakultät

der Ludwig-Maximilians-Universität München

vorgelegt von

Yiyang Wu

aus

Anhui, VR China

Jahr

2026

Mit Genehmigung der Medizinischen Fakultät der
Ludwig-Maximilians-Universität München

Erstes Gutachten:	Priv. Doz. Dr. Thomas Köglsperger
Zweites Gutachten:	Prof. Dr. Jochen Herms
Drittes Gutachten:	Priv. Doz. Dr. Sven Lammich

Dekan: Prof. Dr. med. Thomas Gudermann

Tag der mündlichen Prüfung: 24.02.2026

Table of Contents

Zusammenfassung

Die Parkinson-Krankheit (PD) ist gekennzeichnet durch die pathologische Aggregation von Alpha-Synuclein (αSyn), was zu einer fortschreitenden Neurodegeneration und ausgeprägten motorischen Symptomen führt. Zunehmende Evidenz legt nahe, dass eine gestörte Proteostase eine zentrale Rolle in der αSyn-Pathogenese spielt. Die insulin-degradierende Endopeptidase (IDE) ist eine Zink-Metalloprotease, die für ihre Funktionen im Insulinstoffwechsel und im Abbau amyloidogener Peptide bekannt ist; ihr Einfluss auf die Aggregation und Toxizität von αSyn ist jedoch bislang nur unzureichend verstanden. Ziel dieser Doktorarbeit war es, die Rolle von IDE bei der Modulation der αSyn-Aggregation, ihre Interaktion mit αSyn sowie die daraus resultierenden Effekte auf die neuronale Lebensfähigkeit zu untersuchen. Anhand humaner LUHMES-Zellmodelle und *Ide*-Knockout-Mausmodellen wurde der Einfluss von IDE auf die Löslichkeit, Aggregationsneigung und Zytotoxizität von αSyn systematisch analysiert. Biochemische Fraktionierungen, Western-Blot-Analysen und Thioflavin-T-Assays zeigten, dass ein IDE-Knockdown sowohl endogenes als auch überexprimiertes αSyn signifikant in detergenz-unlösliche Fraktionen verschob und die Bildung β-Faltblatt-reicher Aggregate verstärkte, ohne die Transkriptionsrate von *SNCA* zu beeinflussen. Zudem erhöhte der IDE-Knockdown die αSyn-induzierte Zytotoxizität, wie durch LDH-Freisetzungsassays belegt wurde. Im Gegensatz dazu reduzierte eine IDE-Überexpression den Anteil unlöslicher αSyn-Fraktionen, hatte jedoch keinen signifikanten Effekt auf die akute αSyn-vermittelte Zytotoxizität. In vivo zeigten explorative Analysen an *Ide*-Knockout-Mäusen nach intrazerebraler Injektion von αSyn-Präfibrillen (PFFs) eine verstärkte αSyn-Pathologie, was die protektive Rolle von IDE gegenüber der αSyn-Aggregation im intakten Nervensystem stützt. Strukturmodellierungen mit AlphaFold 3 sowie Co-Immunpräzipitationsassays lieferten übereinstimmende Hinweise auf eine direkte Interaktion zwischen IDE und αSyn. Insgesamt identifizieren diese Ergebnisse IDE als einen wesentlichen Modulator der αSyn-Aggregation

und legen nahe, dass ein IDE-Mangel zur Progression der PD-Pathologie beitragen kann. IDE erscheint damit als vielversprechendes therapeutisches Ziel; der Erhalt bzw. die Steigerung der IDE-Expression/IDE-Spiegel könnte zur Stabilisierung der neuronalen Proteostase beitragen. Die Befunde schlagen eine Brücke zwischen metabolischen und neurodegenerativen Prozessen und liefern eine fundierte Grundlage für die Weiterentwicklung IDE-zentrierter Therapieansätze bei PD.

Abstract

Parkinson's disease (PD) is characterized by pathological aggregation of alpha-synuclein (αSyn), leading to progressive neurodegeneration and debilitating motor symptoms. Accumulating evidence suggests impaired proteostasis plays a pivotal role in αSyn pathology. Insulin-degrading enzyme (IDE) is a zinc metalloprotease known for its roles in insulin metabolism and degradation of amyloidogenic peptides, but its influence on αSyn aggregation and toxicity remains poorly understood. This doctoral research aimed to elucidate the role of IDE in modulating αSyn aggregation, its interaction mechanism with αSyn, and the resultant effects on neuronal viability. Utilizing Lund human mesencephalic (LUHMES) neuronal cells and *Ide* knockout (KO) mice, the study systematically assessed IDE's impact on αSyn solubility, aggregation propensity, and cytotoxicity. Biochemical fractionation, Western blot, and Thioflavin T assays demonstrated that IDE knockdown significantly shifted endogenous and overexpressed αSyn towards detergent-insoluble fractions, increasing β-sheet-rich aggregates without altering *SNCA* transcription levels. IDE knockdown also exacerbated αSyn-induced cytotoxicity, as evidenced by lactate dehydrogenase (LDH) release assays. Conversely, IDE overexpression decreased the insoluble αSyn fraction but did not significantly mitigate acute αSyn-induced cytotoxicity. In pilot in vivo analyses using *Ide* KO mice, IDE deficiency enhanced αSyn pathology following intracerebral injection of αSyn preformed fibrils (PFFs), supporting a protective role of IDE against αSyn aggregation in intact neural systems. Structural modeling with AlphaFold 3, together with co-immunoprecipitation (Co-IP) assays, provided converging evidence for a direct interaction between IDE and αSyn. Collectively, these results identify IDE as a crucial modulator of αSyn aggregation, implicating IDE deficiency in the progression of PD pathology. This study highlights IDE as a promising therapeutic target for PD, suggesting that maintaining IDE function or increasing IDE levels could offer protective benefits by preserving neuronal proteostasis. The findings bridge

metabolic and neurodegenerative processes, offering a compelling rationale for further exploration of IDE-centered therapeutic strategies in PD.

List of Figures

List of Abbreviations

AAV	Adeno-associated virus
AV	Adenovirus
Aβ	Amyloid-beta
BCA	Bicinchoninic Acid
BSA	Bovine Serum Albumin
CMA	Chaperone-mediated Autophagy
CNS	Central nervous System
Co-IP	Co-immunoprecipitation
ddPCR	Droplet Digital PCR
Dibutyryl cyclic-AMP	N6,2'-O-Dibutyryladenosine 3',5'-cyclic Monophosphate Sodium Salt
DIV	Days In Vitro
DMSO	Dimethyl Sulfoxide
DMEM	Dulbecco's Modified Eagle Medium
DPBS	Dulbecco's Phosphate-Buffered Saline
DSS	Disuccinimidyl Suberate

DTT	Dithiothreitol
ER	Endoplasmic Reticulum
FGF	Fibroblast Growth Factor
GDNF	Glial cell line-Derived Neurotrophic Factor
GAPDH	Glyceraldehyde 3-phosphate Dehydrogenase
GFP	Green Fluorescent Protein
GLP-1	Glucagon-like Peptide-1
HRP	Horseradish Peroxidase
IAPP	Islet Amyloid Polypeptide
Ide	Mouse insulin-degrading enzyme gene
IDE	Human insulin-degrading enzyme gene
IDE	Insulin-degrading Enzyme
IGF	Insulin-like Growth Factor
KD	Knockdown
KO	Knockout
LBs	Lewy Bodies
LDH	Lactate Dehydrogenase

LNs	Lewy Neurites
LRRK2	Leucine-Rich Repeat Kinase 2
LUHMES	Lund Human Mesencephalic
MOI	Multiplicity of Infection
NAC	Non-Aβ Component
OB	Olfactory Bulb
OE	Overexpression
PBS	Phosphate-buffered Saline
PD	Parkinson's Disease
PFA	Paraformaldehyde
PFFs	Preformed Fibrils
PINK1	PTEN-induced Kinase 1
PVDF	Polyvinylidene Difluoride
PLO	Poly-L-ornithine
pS129	Phosphorylated Ser129
PVDF	Polyvinylidene Difluoride
SDS	Sodium Dodecyl Sulfate

SEM	Standard Error of the Mean
siRNA	Small Interfering RNA
SNCA	Human α-synuclein gene
SNpc	Substantia Nigra Pars Compacta
T2D	Type 2 Diabetes
TBST	Tris-buffered Saline with Tween-20
ThT	Thioflavin T
TIF	Triton X-insoluble Fraction
TSF	Triton X-soluble Fraction
UPR	Unfolded Protein Response
UPS	Ubiquitin–proteasome System
WT	Wild-type
αSyn	Alpha-synuclein

1. Introduction

1.1 Clinical features and burden of Parkinson's disease

Parkinson's disease (PD) is the second most common neurodegenerative disorder after Alzheimer's disease and the most prevalent movement disorder worldwide (1,2). Clinically, PD is characterized by bradykinesia (slowness of movement) accompanied by at least one of rest tremor or muscle rigidity, often with postural instability in later stages (3). These cardinal motor symptoms result primarily from progressive degeneration of dopaminergic neurons in the substantia Nigra pars compacta (SNpc) and consequent striatal dopamine depletion (4). In addition to motor manifestations, PD patients frequently develop a range of non-motor symptoms – including constipation, anosmia, depression, REM sleep behaviour disorder, autonomic dysfunction, pain, and cognitive impairment – which can precede motor onset by years (5). The pathological hallmarks of PD are the presence of Lewy bodies (LBs) and Lewy neurites (LNs) within affected neurons. These intraneuronal inclusions consist largely of aggregated α-synuclein (αSyn) along with other proteins such as ubiquitin and neurofilaments (4,6). Pathologically, by the time motor symptoms emerge, substantial neuronal loss has already occurred in the SNpc, historically estimated at 50–70% cell loss, though newer evidence suggests early synaptic dysfunction may play a key role before massive cell death (7,8). The temporal relationship between clinical manifestations and underlying neuropathology in PD is illustrated (**Figure 1**). Clinically, non-motor symptoms typically precede motor symptoms by several years, corresponding with the progressive pathological spread of LBs described by Braak staging.

PD imposes a growing public health burden. Its prevalence increases with age, affecting over 1% of people over 60 years old and up to 4% over 85 years old (3). With global population

aging, PD cases have risen dramatically: from 1990 to 2015, the number of people with PD doubled to over 6 million, and it is projected to double again to >12 million by 2040 (9). Indeed, PD is now recognized as the world's fastest-growing neurodegenerative disease (10). This rising prevalence has been attributed not only to longer lifespans but also to possible increases in environmental risk exposures and declining smoking rates (smoking has a protective association) (11). The etiology of PD is multifactorial: most cases are sporadic and likely result from an interplay of aging, genetic susceptibility, and environmental factors (8). Established risk factors include pesticide exposure (e.g. rural living, well-water consumption), prior head injury, and certain genetic mutations, while protective factors include smoking and coffee consumption (12). Approximately 5–10% of PD is familial, caused by single-gene mutations, whereas the remaining sporadic cases may be influenced by many low-risk gene variants (13,14). Genome-wide association studies have identified over 90 risk loci for PD, but these explain only 16–36% of heritable risk, underscoring the importance of non-genetic contributors (14). In sum, PD is a progressive, heterogeneous syndrome with a substantial and increasing global burden, motivating intense research into its pathogenic mechanisms and disease-modifying therapies.

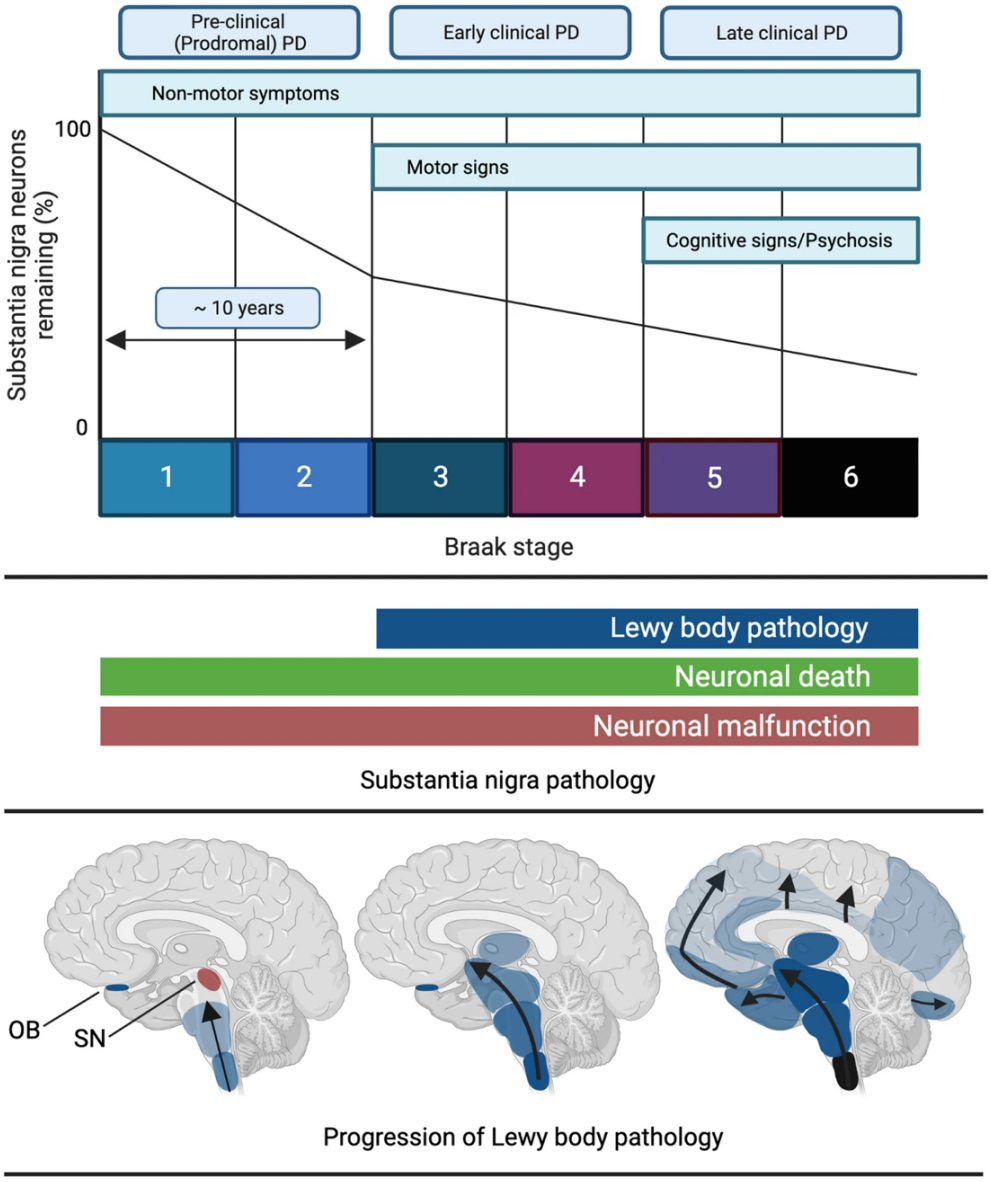

Figure 1. Disease progression in PD and associated neuropathological staging.

Schematic overview illustrating the relationship between clinical progression and neuropathological stages of PD. The upper panel shows the emergence of non-motor symptoms, motor signs, and cognitive impairment across Braak stages 1 to 6, alongside progressive dopaminergic neuron loss in the Substantia Nigra (SN). The middle panel represents the temporal sequence of Lewy body formation, neuronal malfunction, and neuronal death. The lower panel depicts the anatomical progression of Lewy body pathology according to Braak's model, starting from the olfactory bulb (OB), extending to the SN, and eventually affecting cortical regions. (*Adapted from Koeglsperger et al., Mol Neurodegener 2023* (4).)

1.2 αSyn structure, aggregation, and propagation

The aggregation of αSyn is central to PD pathology (**Figure 2**). αSyn is a 140-amino-acid neuronal protein that is abundantly expressed at presynaptic terminals and normally thought to be involved in synaptic vesicle regulation and neurotransmitter release (15,16). Structurally, αSyn is an intrinsically disordered protein in solution, lacking a stable folded structure (17). It is composed of three distinct domains: an N-terminal lipid-binding region (residues 1–65) containing imperfect KTKEGV repeats, a central hydrophobic domain known as the non- Aβ component (NAC, residues 66–95), and a highly acidic C-terminal tail (residues 96–140) (18). The N-terminus can adopt an α-helical conformation upon binding to phospholipid membranes (for example, on synaptic vesicles), and all known familial PD point mutations in *SNCA* (e.g. A53T, A30P, E46K, H50Q, G51D) occur within this N-terminal domain (19). These mutations are believed to promote misfolding or oligomerization of αSyn, leading to early-onset autosomal dominant PD (20). The central NAC domain is crucial for aggregation propensity – it tends to form β-sheet-rich structures that drive the self-assembly of αSyn into fibrils (21). The C-terminal domain, rich in acidic residues, modulates αSyn's interactions with other proteins and metal ions and can influence aggregation kinetics by stabilizing the soluble state (22). Notably, the C-terminus of αSyn is a site of various post-translational modifications (phosphorylation, truncation, nitration) that can affect its aggregation and toxicity (23).

In its native state, αSyn is largely cytosolic and presynaptic, and may function as a chaperone for SNARE-complex assembly, thereby facilitating synaptic vesicle fusion and neurotransmitter release (24). However, under pathological conditions, αSyn misfolds and aggregates into oligomers and insoluble fibrils. Aggregated αSyn is the major constituent of LBs and LNs in PD brains (25) (**Figure 2**). The aggregation of αSyn from soluble monomers into oligomers, protofibrils, and mature fibrils is a hallmark of PD pathology. These fibrillar

structures ultimately accumulate into LBs, the pathological hallmark of PD. This stepwise process—beginning with monomeric αSyn, progressing through oligomeric intermediates, and culminating in fibril and Lewy body formation—is central to disease progression. Notably, αSyn can propagate between neurons in a prion-like manner, contributing to the spatiotemporal spread of pathology across the brain. There is increasing evidence that small, soluble oligomers are particularly neurotoxic, capable of disrupting cell membranes and synaptic function (26,27). For example, certain oligomeric conformations of αSyn can form pore-like complexes in lipid membranes, causing calcium dysregulation and cellular injury (11). Fibrillar αSyn, while a marker of disease, may be less toxic per unit mass than oligomers, though fibrils can release oligomeric fragments that propagate toxicity (28). Pathological αSyn in LBs is often heavily phosphorylated at serine-129 and truncated, modifications that may accelerate aggregation or impair clearance (29).

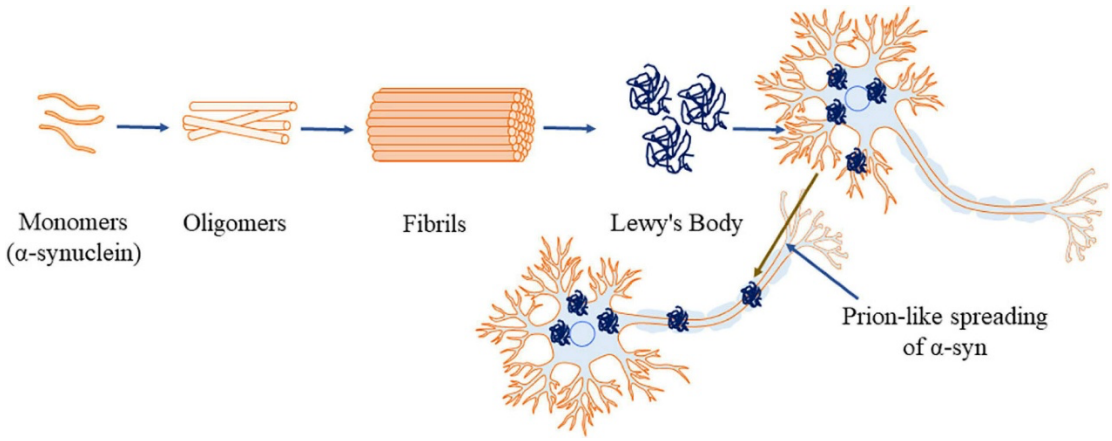

Figure 2. Pathological aggregation and spreading of αSyn.

Monomeric αSyn forms oligomers and fibrils, leading to Lewy body formation. Aggregates can propagate between neurons in a prion-like manner, contributing to disease progression. (*Adapted from Ray et al., Front Cell Dev Biol 2021* (30).)

A remarkable aspect of αSyn pathology is its spatiotemporal progression (′spread′) in the nervous system. Braak and colleagues first proposed that misfolded αSyn may propagate in a

prion-like fashion along interconnected neural pathways, contributing to PD's progressive spread of pathology from peripheral entry sites to the brain. According to Braak staging, αSyn pathology often first appears in the olfactory bulb and enteric nervous system (dorsal motor nucleus of the vagus) and then ascends to the brainstem and midbrain, eventually reaching cortical areas in late disease (31). This pattern suggests a cell-to-cell transmission of pathogenic αSyn. Indeed, experimental studies have shown that αSyn fibrils can be taken up by neurons and seed the aggregation of endogenous αSyn, which then spreads trans-synaptically to anatomically connected regions (32). Pathogenic αSyn can be released from neurons via exosomes or other secretory mechanisms and taken up by neighbouring cells, effectively disseminating the pathology in a template-directed manner (33,34), as illustrated in the intracellular trafficking pathways of αSyn (**Figure 3**). This prion-like behaviour of αSyn is supported by animal models: injection of PFFs into the brain or periphery of rodents induces progressive Lewy body-like inclusion formation along neural pathways and dopamine neuron loss, recapitulating key features of PD (31,35). The propagation hypothesis has significant implications: it suggests that targeting αSyn spreading or seeding could slow disease progression (36). Efforts are underway to develop immunotherapies and small molecules to neutralize extracellular αSyn or prevent its uptake and aggregation in recipient cells (37,38) (**Figure 3**).

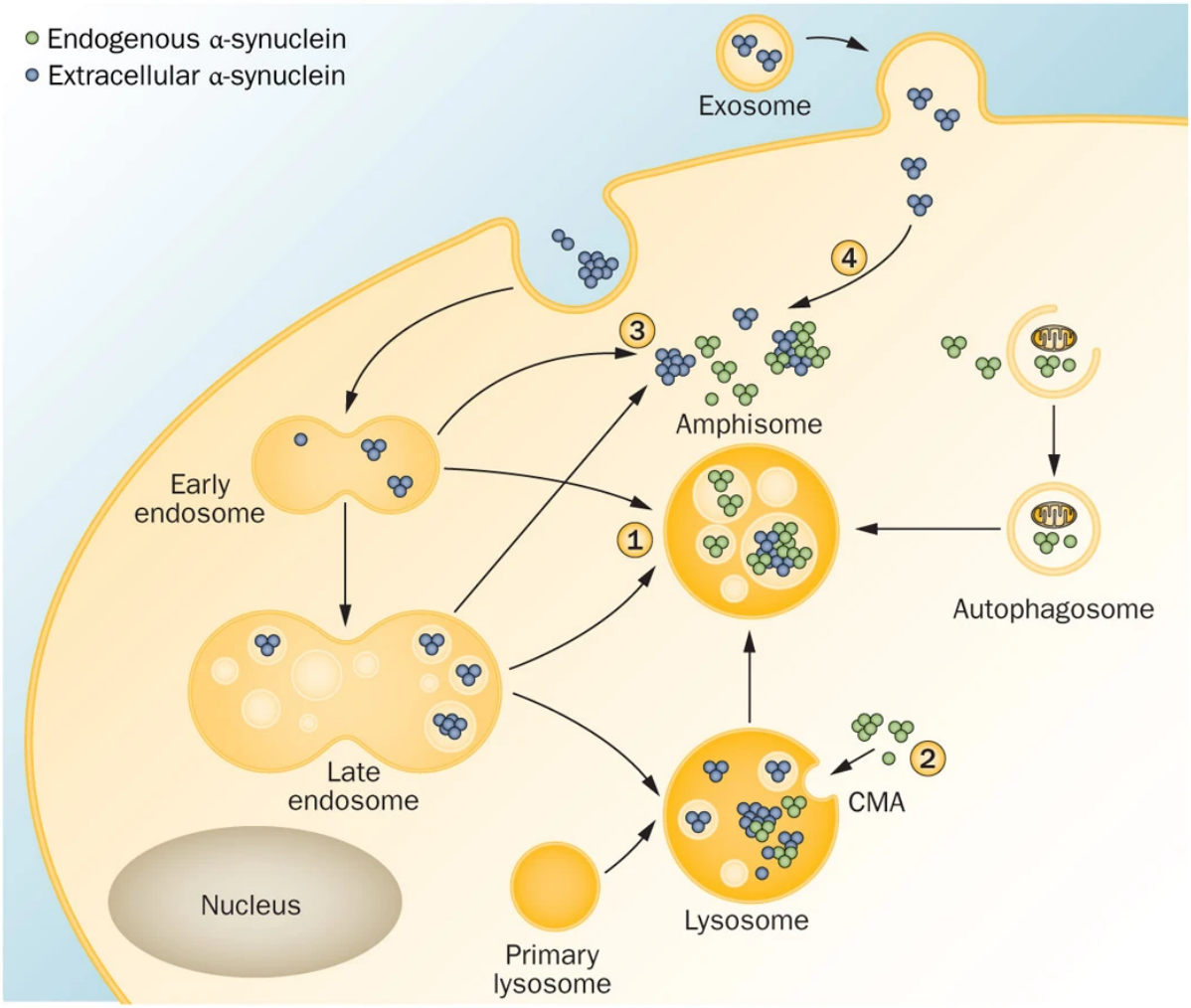

Figure 3. Intracellular trafficking and degradation of αSyn.

Endogenous (green) and extracellular (blue) αSyn are internalized via endocytosis and processed through lysosomal degradation, chaperone-mediated autophagy (CMA), or secreted via exosomes. These pathways regulate αSyn homeostasis and intercellular propagation. *(Adapted from Lee et al., Nat Rev Neurol 2014* (34)*.)*

In summary, αSyn is a neuronal protein with a propensity to misfold into toxic aggregates. Its central role in PD is evident from genetic, pathological, and experimental data linking αSyn aggregation to neurodegeneration. The familial PD cases caused by *SNCA* mutations or multiplications demonstrate that aberrant αSyn can initiate the disease (8,39). In sporadic PD, αSyn pathology is a defining feature, and its spread correlates with disease progression and clinical severity. Understanding the factors that regulate αSyn aggregation and clearance is

therefore critical for elucidating PD pathogenesis and identifying disease-modifying therapies (40).

1.3 Proteostasis and protein clearance pathways in PD

The accumulation of misfolded αSyn in PD reflects an underlying failure of protein homeostasis (proteostasis). Under normal conditions, cells rely on several proteostatic mechanisms to refold or degrade aberrant proteins, including molecular chaperones, the ubiquitin-proteasome system (UPS), and the autophagy-lysosomal pathways (41,42) (**Figure 4**). In neurons, which are post-mitotic and long-lived, efficient clearance of misfolded or aggregated proteins is especially vital. Converging evidence implicates proteostasis impairment in the pathogenesis of PD and other synucleinopathies (43).

Ubiquitin-Proteasome System (UPS): The UPS is responsible for the targeted degradation of short-lived or misfolded proteins in the cytosol and nucleus. Substrates tagged with ubiquitin chains are recognized and proteolyzed by the 26S proteasome complex (**Figure 4**). In PD, early studies noted that LBs contain ubiquitin and proteasomal subunits, hinting at UPS dysfunction (44). Pharmacological inhibition of the proteasome in cell and animal models leads to the accumulation of αSyn and neurodegeneration, mimicking PD-like changes (45,46). However, the UPS has limited capacity to degrade large protein aggregates. αSyn fibrils exhibit resistance to proteasomal degradation (47). Instead, they may sequester or overload proteasomes, exacerbating proteostasis stress. Some familial PD genes point to UPS defects: for example, mutations in PARK2 (Parkin) – an E3 ubiquitin ligase – cause autosomal recessive PD by impairing ubiquitination of substrates, and parkin substrates can accumulate in those cases (48).

Despite these links, UPS alone cannot clear large αSyn aggregates, suggesting other pathways are crucial for handling αSyn pathology (49).

Autophagy-Lysosomal Pathways: Neurons heavily rely on autophagy to degrade long-lived proteins, protein aggregates, and damaged organelles. There are three major forms of autophagy: macroautophagy, chaperone-mediated autophagy (CMA), and microautophagy. Macroautophagy involves sequestration of cytosolic cargo into double-membraned autophagosomes which then fuse with lysosomes. CMA is a selective pathway where specific proteins bearing a KFERQ-like motif are recognized by chaperones (Hsc70) and delivered directly across the lysosome membrane via the receptor LAMP2A (50,51). Notably, wild-type (WT) αSyn is a substrate of CMA: it contains a CMA-targeting motif and can be translocated into lysosomes for degradation (**Figure 4**). However, pathogenic αSyn variants (A53T, A30P) and possibly oligomeric αSyn can bind to LAMP2A but fail to properly translocate, thereby acting as blockers of CMA. Cuervo et al. (2004) demonstrated that mutant αSyn binds the CMA receptor tightly and jams the translocation mechanism, inhibiting its own degradation and that of other CMA substrates (43). This “clogging” of CMA by mutant or aggregated αSyn could contribute to a toxic positive feedback loop: as CMA activity declines, more αSyn accumulates, which in turn further impairs CMA. Consistent with this, post-mortem PD brains show reductions in LAMP2A and other CMA components, suggesting CMA dysfunction in disease (52,53).

Macroautophagy is also implicated in αSyn clearance. αSyn aggregates and damaged organelles are engulfed in autophagosomes and delivered to lysosomes. If autophagy is impaired, αSyn can accumulate. Several PD-related genes converge on autophagy-lysosomal biology. For instance, biallelic mutations in GBA (glucocerebrosidase) – a lysosomal enzyme – are the most frequent genetic risk factor for PD, increasing risk approximately 5-fold (54,55).

GBA mutations cause lysosomal dysfunction and are thought to hinder the clearance of αSyn, explaining the association between Gaucher disease (lysosomal storage disorder due to GBA loss) and parkinsonism. Likewise, LRRK2 (leucine-rich repeat kinase 2), mutated in autosomal dominant PD, has been shown to perturb autophagy and endosomal trafficking when mutated, and its inhibition can enhance autophagic flux (55,56). Loss-of-function mutations in the genes PINK1 and PARKIN impair mitophagy (autophagic removal of damaged mitochondria), linking defective organelle clearance to early-onset PD (57). In sporadic PD brains, evidence of accumulated autophagic vacuoles and substrates suggests that macroautophagy may be overtaxed or inefficient (58). Experimental support for autophagy's role comes from studies showing that enhancing autophagy can reduce αSyn aggregates: for example, pharmacological inducers of autophagy or genetic upregulation of autophagy-related proteins promote clearance of mutant αSyn and protect neurons in cellular and animal models. By contrast, impairing autophagy (e.g. via knockout of autophagy genes or using inhibitors like chloroquine) exacerbates αSyn accumulation and toxicity (59,60). Overall, the autophagy-lysosome system is a critical defence against αSyn proteotoxicity, and its dysfunction is a key feature of PD.

Protein-Folding Chaperones: In addition to degradation pathways, molecular chaperones (like heat shock proteins Hsp70, Hsp90, etc.) assist in refolding misfolded proteins and preventing aggregation. In PD models, overexpression of certain chaperones (e.g. Hsp70) can reduce αSyn aggregation and neuronal death (61). Conversely, overwhelming the chaperone capacity (due to excessive misfolded proteins) can trigger endoplasmic reticulum (ER) stress and the unfolded protein response (UPR) (62). Markers of chronic ER stress and UPR activation have been observed in PD brains, indicating that proteostasis in the secretory pathway is also disrupted. Chronic stress may shift the balance from protective UPR signalling to pro-apoptotic pathways, contributing to neuron loss. Modulating chaperone activity is being explored as a therapeutic angle – for example, small molecules that act as "chemical chaperones"

or enhance endogenous chaperone expression might help maintain αSyn in a soluble, non-toxic state (23,63).

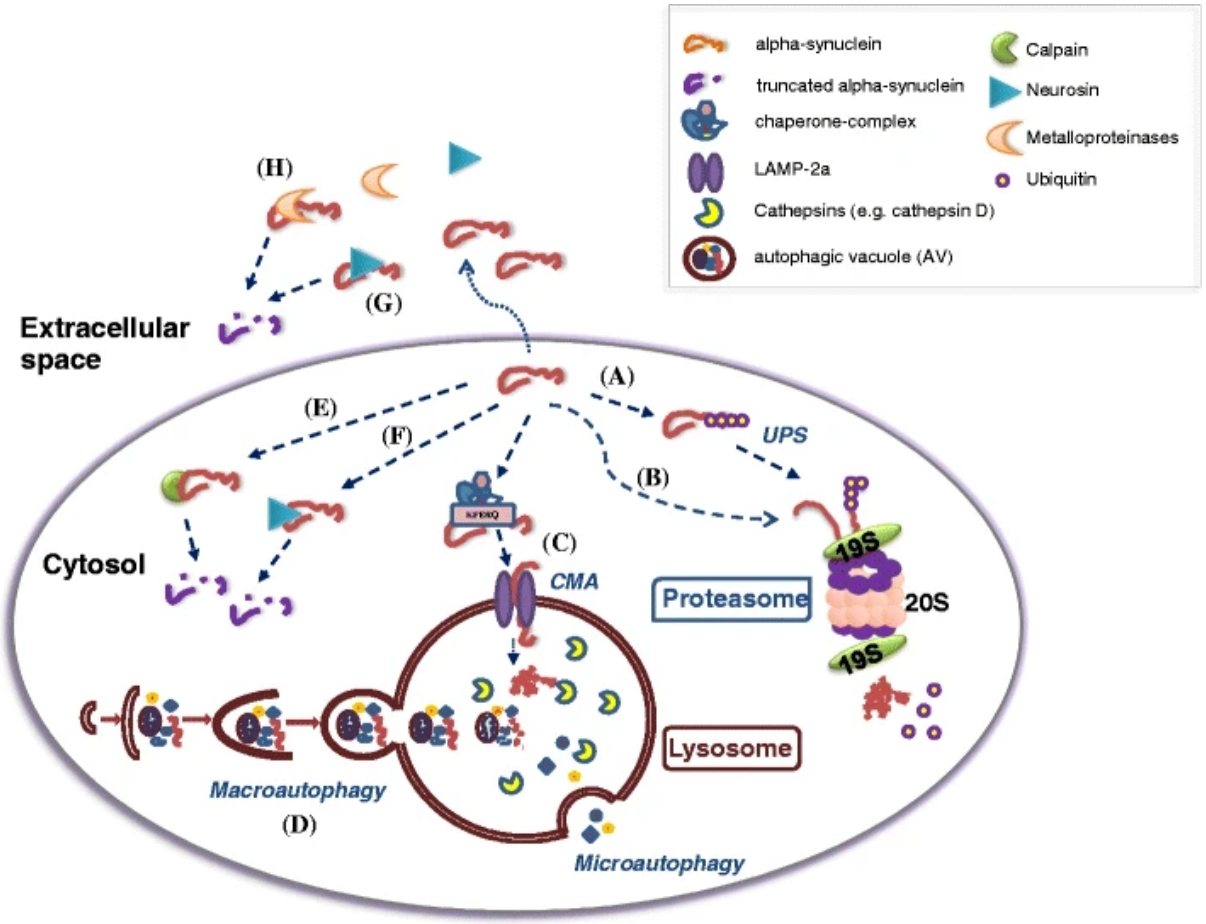

Figure 4. Proteostasis pathways involved in αSyn clearance, including the UPS, CMA, macroautophagy, and extracellular protease-mediated degradation.

A–H denote: (A) ubiquitin-dependent proteasomal degradation (UPS); (B) ubiquitin-independent proteasomal degradation; (C) chaperone-mediated autophagy (CMA) via LAMP-2A; (D) macroautophagy, in which cargo is sequestered in autophagic vacuoles and degraded in lysosomes; (E) intracellular cleavage of αSyn by calpains; (F) intracellular cleavage by neurosin/KLK6; (G) extracellular cleavage by secreted neurosin; (H) extracellular cleavage by metalloproteinases. Abbreviations: αSyn, alpha-synuclein; UPS, ubiquitin–proteasome system; CMA, chaperone-mediated autophagy; LAMP-2A, lysosome-associated membrane protein-2A; AV, autophagic vacuole. *(Adapted from Xilouri et al., Mol Neurobiol 2013* (42)*).*

In summary, a breakdown of protein clearance mechanisms – whether due to genetic mutations or age-related decline – appears to underlie the pathological accumulation of αSyn in PD. The UPS is inefficient at handling large αSyn aggregates, placing greater reliance on lysosomal pathways for disposal of this protein. Both CMA and macroautophagy play major roles in αSyn turnover: WT αSyn can be degraded by CMA and macroautophagy (62,63), and inhibition of either pathway leads to αSyn accumulation. Indeed, αSyn has been shown to be degraded by chaperone-mediated autophagy and macroautophagy in neuronal cells (64,65). In PD, these clearance systems are often found impaired, creating a permissive environment for αSyn misfolding and aggregation. This has motivated trials of therapies aimed at boosting proteostasis in PD – such as small-molecule enhancers of autophagy, inhibitors of αSyn aggregation, and upregulators of chaperones. Strengthening the cell's proteostatic capacity could, in principle, slow or prevent the accumulation of toxic αSyn species and thereby modify the disease course. One promising avenue is the upregulation of CMA: studies in cellular models have shown that enhancing CMA (for instance, by overexpressing LAMP2A or pharmacologically activating CMA) leads to increased clearance of αSyn and reduced toxicity (64). Similarly, induction of macroautophagy via mTOR inhibition or other routes has been reported to clear aggregate-prone proteins and provide neuroprotection in PD models (66). These approaches underscore the critical link between proteostasis and PD pathogenesis, and they set the stage for exploring specific proteostatic modulators – such as IDE – in the context of αSyn aggregation.

1.4 IDE and its relevance to αSyn biology

IDE, also known as insulysin, is a zinc-dependent metalloprotease that has emerged as an intriguing player at the intersection of metabolic disease and neurodegeneration (67). IDE was

initially discovered over 70 years ago as an enzyme capable of degrading insulin in liver extracts (68,69). It is an approximately 110 kDa thiol metalloprotease found predominantly in the cytosol, with additional localization to peroxisomes and certain extracellular locales. Notably, IDE has an unusual 'closure' mechanism, encapsulating its substrates within an internal chamber for proteolysis (70). Despite its name, IDE has a broad substrate spectrum and is not specific to insulin. Notably, IDE can degrade several amyloidogenic peptides, including amyloid-β (Aβ) of Alzheimer's disease and amylin (islet amyloid polypeptide, IAPP) of type 2 diabetes (71,72). IDE's known substrates are typically peptides of up to ~50 amino acids; it efficiently cleaves insulin (51 amino acids) and Aβ (40–42 amino acids) into non-toxic fragments. Because of its ability to catabolize Aβ, IDE has been studied in Alzheimer's disease models: IDE deficiency in mice leads to elevated brain Aβ levels and accelerated plaque formation, whereas increasing enhancing IDE's proteolytic activity reduces Aβ accumulation (73,74). Furthermore, genetic association studies have linked polymorphisms in the IDE gene to both type 2 diabetes (T2D) and Alzheimer's disease, highlighting its importance in metabolic and proteostatic processes (75).

The connection between IDE and PD is a more recent and evolving area of research. Although αSyn (140 aa) is much larger than IDE's typical substrates, evidence suggests that IDE can interact with αSyn and influence its aggregation behaviour. The first clues came from cross-disease observations: T2D and PD often co-occur, and epidemiological studies indicate that T2D is associated with an elevated risk of developing PD (on the order of 1.2–1.8-fold increased risk) (76,77). IDE, being a key enzyme in insulin metabolism, was a candidate link between these conditions. Indeed, genome-wide association studies identified IDE (on chromosome 10q23) as a T2D-associated gene that also might affect β-cell function (75). In a landmark study, Sharma et al. (2015) demonstrated in vitro that IDE can bind to αSyn and prevent its fibrillization without actually digesting it (72). In their experiments, sub-

stoichiometric amounts of IDE (i.e., IDE present in much lower molar ratio than αSyn) effectively inhibited the conversion of αSyn monomers/oligomers into amyloid fibrils. This anti-aggregation effect was shown to be "nonproteolytical," meaning IDE did not cleave αSyn in this context but likely formed a stable complex with it. By binding αSyn oligomers, IDE rendered them inert or unable to elongate into fibrils. Intriguingly, the interaction was mutually beneficial: binding of αSyn oligomers allosterically increased IDE's protease activity towards a small fluorogenic substrate, suggesting that αSyn (particularly its acidic C-terminal region) can activate IDE. A follow-up study pinpointed that the C-terminus of αSyn (residues 96–140) is responsible for this activation of IDE and the prevention of aggregation (22). Truncated αSyn lacking the C-terminus failed to activate IDE or be protected from aggregation, whereas a peptide corresponding to αSyn's C-terminal 44 amino acids could mimic the full-length protein's effects. This implies an electrostatic interaction between αSyn's negatively charged C-tail and a basic "exosite" on IDE that modulates its activity. These in vitro findings support a model in which IDE serves as a proteostasis guardian: it can sequester aggregation-prone proteins like αSyn and Aβ, either degrading them if they fit into its catalytic chamber or, if they are too large, holding them in a complex that prevents further aggregation. By doing so, IDE may reduce the formation of toxic oligomers and fibrils in cells (78).

Beyond in vitro biochemical analyses, emerging evidence from animal models and post-mortem human tissues reinforces IDE's role in modulating αSyn. A 2013 study by Steneberg et al. examined mice with a knockout (KO) of the Ide gene and found an unexpected phenotype in pancreatic β-cells: IDE deficiency led to accumulation of αSyn in islets, accompanied by impaired insulin secretion and reduced autophagic flux. Normally, IDE and αSyn levels in β-cells were inversely correlated (more IDE, less αSyn). In *Ide* KO mice, αSyn protein levels were significantly increased in pancreatic islets, and importantly, the researchers showed that IDE can form stable complexes with αSyn in these cells. They also observed that human T2D

islets (which often have reduced IDE expression) showed elevated αSyn levels, paralleling the mouse findings. Conversely, overexpression of αSyn in otherwise normal β-cells impaired insulin secretion and autophagy, indicating that too much αSyn is detrimental to β-cell function (75). This study extended the relevance of αSyn beyond neurons, identifying it as a factor in β-cell biology, and crucially identified IDE as a regulator that keeps αSyn levels in check in cells. These findings hint that in tissues where IDE is low or absent, αSyn might accumulate and cause dysfunction, an observation that likely also applies to neurons.

Relatively few studies have directly measured IDE in the context of PD brains or models until now. One clinical study measured IDE levels in the serum of PD patients and found no significant difference compared to healthy controls (79). However, since peripheral IDE levels may not accurately reflect its activity in the central nervous system (CNS), and post-mortem brain analyses of IDE in PD are not well documented, the implications of these findings are unclear. Given IDE's known role in degrading Aβ, we hypothesized that enhancing IDE's non-proteolytic αSyn-binding (holdase) function could also promote the clearance of αSyn or mitigate its aggregation. On the other hand, IDE's multifunctionality means that any change in its activity could have broad effects. For instance, complete loss of IDE in mice causes not only amyloid protein accumulation but also metabolic disturbances like glucose intolerance and hyperinsulinemia (due to impaired insulin degradation). Thus, IDE sits at a crossroads of metabolic and proteostatic pathways: it regulates insulin and glucose metabolism and concurrently patrols for amyloidogenic proteins. This dual role raises interesting questions for PD: could peripheral metabolic conditions (like insulin resistance or diabetes) influence αSyn aggregation in the brain? There is evidence that insulin resistance and hyperglycemia can worsen neurodegenerative pathology (80). Some studies even suggest that anti-diabetic medications might modulate PD risk – for example, patients on glucagon-like peptide-1 agonists (GLP-1 analogs) showed lower PD incidence in epidemiological studies, whereas

those on certain other medications like metformin had a slight increase in PD risk. While these associations involve complex mechanisms, they underscore a potential interplay between systemic metabolic enzymes (like IDE) and neurodegenerative processes (81).

In summary, IDE has known neuroprotective capabilities against amyloidogenic peptides: it degrades or binds factors like Aβ, IAPP, and now αSyn, to prevent toxic accumulation. IDE's emerging relevance in αSyn biology is supported by in vitro biochemical data and in vivo observations (72,75). These findings raise the possibility that IDE in the brain could act as a modifier of αSyn pathology – potentially slowing aggregation in normal conditions, or, if IDE levels or IDE function decline (for example with aging or genetic variation), allowing more rapid αSyn accumulation. However, this hypothesis needed to be rigorously tested in neuronal models of PD, as prior studies had not directly examined whether manipulating IDE levels in neurons would influence αSyn aggregation or neurotoxicity in the context of PD.

1.5 The Role of IDE in αSyn Pathology: Hypothesis and Research Objectives

1.5.1 Scientific Rationale

Given the evidence above, we hypothesized that IDE might function as a key modulator of αSyn proteostasis in the nervous system. If IDE normally binds or degrades αSyn to prevent its aggregation (72), then reducing IDE levels should lead to greater αSyn aggregation and associated cellular toxicity. Conversely, increasing IDE might enhance the clearance or neutralization of αSyn and protect against its pathogenic effects. This hypothesis is compelling because it connects a metabolic enzyme with neurodegeneration, potentially explaining links between conditions like diabetes and PD. It also opens a novel therapeutic angle: if boosting IDE function in the brain can reduce αSyn aggregates, IDE or its regulators could be targets

for disease-modifying therapies in PD. However, prior to this work, evidence for IDE's role in αSyn aggregation in neuronal systems and animal models was lacking. Most insights came from test-tube assays or non-neuronal cells (e.g., β-cells). It remained to be determined whether altering IDE expression in a neuronal context (either in cultured neurons or in the brain) would indeed impact αSyn aggregation, αSyn-induced neurotoxicity, and overall PD-like pathology. Moreover, the mechanism by which IDE interacts with αSyn in cells needed clarification – e.g., does IDE physically bind αSyn in living neurons, and is this interaction relevant under physiological conditions or only when IDE is overexpressed?

1.5.2 Research Objectives

Objective 1 – IDE Modulation in Neuronal αSyn Aggregation

Determine the effect of IDE knockdown or overexpression on αSyn aggregation in neuronal cell models**.** We utilized human neuron-like cells overexpressing αSyn (to mimic the elevated αSyn of PD) and manipulated IDE levels via RNA interference (siRNA knockdown) and viral vector overexpression. We hypothesized that IDE knockdown would exacerbate αSyn aggregation, whereas IDE overexpression would attenuate it. Biochemically, we planned to assess αSyn accumulation in detergent-soluble vs. insoluble fractions to quantify aggregation, and to verify changes by techniques like Western blot and possibly aggregation-specific assays.

Objective 2 – IDE Deficiency in Mouse Models of PD

Examine the role of IDE in αSyn pathology in vivo using mouse models. We took advantage of transgenic/viral models of αSyn aggregation in mice to test if IDE deficiency worsens pathology. Specifically, we proposed to use *Ide* KO mice and introduce αSyn pathology either by injecting PFFs into the brain or by using an adeno-associated virus (AAV) to overexpress αSyn in the brain. We expected that mice lacking IDE would show greater accumulation of

pathogenic αSyn (including insoluble aggregates and phosphorylated αSyn) compared to WT mice when challenged with these PD models. This aim would establish a causative link between IDE and αSyn aggregation in vivo. We also aimed to check if IDE deletion alone (without an exogenous αSyn challenge) leads to any αSyn alterations or neurodegenerative changes with aging.

Objective 3 – IDE–αSyn Interaction Mapping

To explore whether IDE and αSyn physically interact and to define the interface of this interaction, we used AlphaFold 3 to predict the structure of the IDE–αSyn complex. The predicted model was subsequently visualized and analyzed using PyMOL to identify key interface residues. Based on these insights, we designed co-immunoprecipitation (Co-IP) experiments in cells co-expressing IDE and αSyn, and considered site-directed mutagenesis to validate the structural predictions. Together, these approaches aimed to clarify whether IDE binds αSyn directly and how this interaction may underlie its modulatory effects.

Objective 4 – Functional Impact on αSyn-Induced Cytotoxicity

Evaluate the functional consequences of IDE modulation on αSyn-induced cytotoxicity. Ultimately, if IDE affects αSyn aggregation, does this translate into differences in neuronal cell survival or toxicity? We addressed this by measuring cell injury in our models. In vitro, we used the LDH release assay to quantify cytotoxicity in neuron-like cells under different conditions: with αSyn overexpression, with IDE knockdown or overexpression, or combinations thereof. Our expectation was that IDE knockdown would exacerbate αSyn-induced cell death, whereas IDE overexpression might rescue cells from αSyn toxicity. Similarly, in vivo, we intended to assess neurodegeneration (for example, loss of dopaminergic neurons in the substantia nigra or markers of apoptosis) in the presence or absence of IDE under αSyn pathological stress. This objective is important for establishing whether modulating

IDE just changes protein aggregation or actually impacts disease-relevant outcomes (neuronal survival and function).

1.5.3 Summary of Study Design

By integrating these aims, our study seeks to comprehensively characterize the role of IDE in the context of PD proteinopathy. In summary, the central question is: Does IDE act as a protective factor that mitigates αSyn aggregation and toxicity, and could its absence tip the balance towards pathology? We approached this by manipulating IDE in cellular and animal models and assessing effects on αSyn aggregation, protein interaction, and cell viability. Confirming IDE's influence on αSyn pathology would not only deepen our understanding of PD mechanisms but also potentially identify IDE as a novel target for therapeutic intervention – for example, via small molecules that enhance IDE function or via gene therapy to boost IDE in the brain. This thesis details the experiments undertaken to answer these questions and discusses the implications of the findings for PD pathogenesis and treatment.

2. Methods

2.1 Cell biology

This section details the cell culture conditions, genetic manipulation protocols, and assay timelines used to assess the effects of IDE modulation on dopaminergic neuronal models. LUHMES cells were employed due to their robust differentiation into mature dopaminergic neurons. The sequence of Small Interfering RNA (siRNA) transfection, adenoviral (AV) transduction, and endpoint analyses such as LDH cytotoxicity, Western blot, and Thioflavin T aggregation assays is illustrated in **Figure 5**.

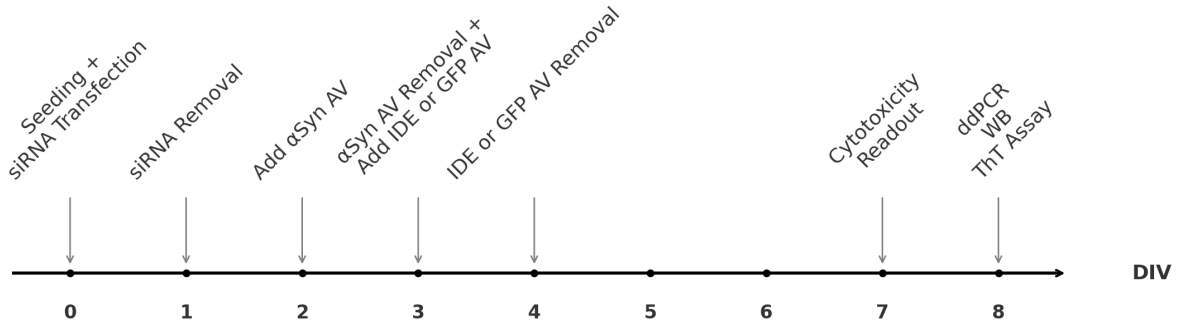

Figure 5. Schematic of the experimental timeline for siRNA transfection, AV treatment, and endpoint assays.

LUHMES cells were transfected with IDE or control siRNA on day 0 (DIV 0; Days In Vitro). αSyn AV was added on DIV 2. On DIV 3, αSyn AV medium was replaced and IDE or GFP AV was added. Viral supernatants were removed on DIV 4. Cytotoxicity assays were performed on DIV 7, and molecular readouts (ddPCR, or ThT assay) were conducted on DIV 8.

2.1.1 Cell culture

LUHMES cells were cultured under standard conditions using Thermo Scientific™ Nunc™ EasYFlask™ for proliferation and Nunc™ Cell-Culture Treated Multidishes for differentiation experiments. All cultures were maintained at 37 °C in a humidified incubator (Thermo Fisher

Scientific) with 5 % CO_2. Prior to cell seeding, culture vessels were coated with 0.1 mg/mL poly-L-ornithine (PLO, Sigma-Aldrich) for 24 h at 37 °C, followed by three washes with DPBS (Thermo Fisher Scientific). For neuronal differentiation, an additional coating with 5 µg/mL bovine fibronectin (R&D Systems) was performed under the same conditions. Cells were maintained in DMEM/F-12 (Sigma-Aldrich) supplemented with 1 % N-2 supplement (Thermo Fisher Scientific) and 0.04 µg/mL recombinant human FGF-basic (Peprotech) during proliferation. To initiate differentiation, the medium was replaced with DMEM/F-12 (Sigma-Aldrich) containing 1 % N-2, 1 µg/mL Tetracycline hydrochloride (Sigma-Aldrich), 0.49 mg/mL dibutyryl cyclic AMP (Sigma-Aldrich), and 2 ng/mL recombinant human GDNF (Bio-Techne). Unless otherwise specified, cells were seeded at a density of 1×10^5 cells/cm² to achieve approximately 50% confluence and differentiated for 6 days in differentiation medium. After 6 days, LUHMES cells acquire a post-mitotic neuronal phenotype with dopaminergic characteristics, providing a suitable model system for downstream applications (82).

2.1.2 Viral vector transduction

To induce viral overexpression of αSyn or GFP (as a control), LUHMES cells were transduced 24 h after plating with AV serotype 5 constructs encoding either αSyn (Ad5-αSyn) or GFP (Ad5-GFP) at a multiplicity of infection (MOI) of 2.15, following previously described procedures (83). For IDE overexpression, custom Ad5-based AVs expressing human IDE fused to EGFP via a flexible linker (IDE-Adv, VectorBuilder, Vector ID: VB240909-1712cvt) or an EGFP-only control virus (Ctrl-Adv, VectorBuilder, Vector ID: VB010000-9299hac) were transduced on the DIV 2 at a MOI of 5 for 24 h. After each viral incubation, the medium was carefully removed, and cells were washed three times with DPBS before fresh differentiation medium was added.

2.1.3 siRNA transfection

For transient knockdown of IDE, LUHMES cells were transfected with Silencer™ Select predefined siRNA targeting human IDE (Thermo Fisher Scientific). Silencer™ Select Negative Control No. 1 siRNA (Thermo Fisher Scientific) was used as a non-targeting control under identical conditions. On DIV 0, 10 µL siRNA (10 µM) and 9 µl Lipofectamine™ RNAiMAX (Thermo Fisher Scientific) were separately diluted in Opti-MEM™ and combined, followed by a 5–15-minute incubation at room temperature to facilitate complex formation. After incubation, the transfection mixture was directly added to each well of a 6-well plate without mixing or pipetting vigorously, to avoid disrupting the formed complexes. Subsequently, 1 mL of LUHMES cell suspension at a density of 1×10^6 cells/mL was gently added to ensure simultaneous seeding and transfection. After 12 hours of incubation, the medium was carefully replaced with fresh differentiation medium.

2.1.4 LDH cytotoxicity assay

Cellular cytotoxicity was assessed using the CytoTox-ONE™ Homogeneous Membrane Integrity Assay (Promega) with minor modifications. LUHMES cells were seeded at a density of 125,000 cells/well in 300 µL of differentiation medium in 48-well plates and differentiated under standard conditions. All treatments were completed by DIV 3, after which the medium in all wells was replaced to standardize LDH accumulation across conditions. The cells were then incubated for an additional 4 days. On day 7, 100 µL of culture supernatant from each well was collected and transferred into a black 96-well plate (Greiner), followed by the addition of 100 µL of CytoTox-ONE™ Reagent (Promega). The plate was gently shaken for 30 seconds and incubated at room temperature (22 °C) for 10 minutes in the dark. To terminate the reaction, 50 µL of Stop Solution was added in the same order as the reagent to ensure equal reaction time. Fluorescence was measured immediately using a microplate reader (ClarioStar, BMG

labtech, Ortenburg, Germany) set at 560 nm excitation and 590 nm emission. Background fluorescence from no-cell controls was subtracted, and percent cytotoxicity was calculated relative to maximum LDH release induced by lysis control.

$$\text{Percent Cytotoxicity} = 100 \times \frac{(\text{Experimental} - \text{Culture Medium Background})}{(\text{Maximum LDH Release} - \text{Culture Medium Background})}$$

2.2 Molecular biology

To evaluate the transcriptional changes of *SNCA* following IDE knockdown, total RNA was extracted from LUHMES cells and reverse-transcribed into complementary DNA (cDNA). Droplet digital PCR (ddPCR) was subsequently performed to quantify *SNCA* mRNA expression.

2.2.1 RNA isolation

Total RNA was extracted from adherent LUHMES cells using the RNeasy Mini Kit (Qiagen) operated on the QIAcube automated workstation (Qiagen). Cells were lysed directly on the culture plate using Buffer RLT supplemented with 1 % β-mercaptoethanol. The lysates were subsequently transferred to RNase-free 2 mL tubes and loaded onto the QIAcube system, which was preloaded with spin columns and filter tips. All subsequent steps—including RNA binding, washing, and elution—were carried out automatically using the standard protocol for cultured cells. RNA was eluted in RNase-free water. RNA concentration was measured using the Qubit™ 3 Fluorometer (Invitrogen, Thermo Fisher Scientific).

2.2.2 Reverse transcription

Equal amounts of total RNA were reverse transcribed into cDNA using the QuantiTect Reverse Transcription Kit (Qiagen) according to the manufacturer's instructions. The RNA concentration was measured using the Qubit™ RNA HS Assay Kit with the Qubit™ 3 Fluorometer (Invitrogen, Thermo Fisher Scientific) and adjusted to match the sample with the lowest concentration to ensure consistent input. To eliminate genomic DNA contamination, RNA samples were first incubated with gDNA Wipeout Buffer at 42 °C for 2 minutes. The reverse transcription reaction was subsequently performed in a final volume of 20 µL containing Quantiscript RT Buffer, RT Primer Mix, and Quantiscript Reverse Transcriptase. Reactions were incubated at 37 °C for 30 minutes, followed by 95 °C for 3 minutes to inactivate the enzyme. Synthesized cDNA was stored at –20 °C until further use.

2.2.3 Digital droplet PCR (ddPCR)

Digital droplet PCR (ddPCR) was performed using the QX200™ Droplet Digital PCR System (Bio-Rad, Hercules, CA, USA) to quantify mRNA expression of *IDE* and *SNCA*. Each 20 µL reaction contained 1 µL cDNA, 1 µL of TaqMan Gene Expression Assay (Hs00610452_m1 for *IDE*, Hs00240906_m1 for *SNCA*; Thermo Fisher Scientific), and 2× ddPCR Supermix for Probes (no dUTP, Bio-Rad). Droplet generation was performed using DG8™ Cartridges, DG8 Gaskets, and Droplet Generation Oil for Probes (all from Bio-Rad), on a QX200 Droplet Generator. Thermal cycling was conducted on a C1000 Touch™ Thermal Cycler with a 96-Deep Well Reaction Module (Bio-Rad) using the following protocol: enzyme activation at 95 °C for 5 min, followed by 40 cycles of 95 °C for 30 s and 60 °C for 1 min, then 4 °C for 5 min and 90 °C for 5 min for signal stabilization. Following amplification, droplets were analyzed using the QX200 Droplet Reader (Bio-Rad). Data acquisition and quantification were performed using QX Manager™ Software (Bio-Rad), with manual adjustment of fluorescence thresholds for accurate quantification. All reactions were run in technical duplicates.

2.3 Intrastriatal PFFs injections

Female *Ide* WT and *Ide* KO mice, 2–3 months old, were used. Mouse α-synuclein PFFs were assembled at 5 mg/mL (37 °C, 1000 rpm, 7 days), quality-checked by Thioflavin-T fluorescence (final 5 μM) and a sedimentation assay (100,000 × g, 30 min), and fragmented immediately before surgery by probe sonication (30 % amplitude, 4 × 15 s; 1 s on/2 s off). Mice received unilateral intrastriatal injections targeting the dorsal striatum (AP +0.2 mm, ML +2.0 mm, DV −3.8 mm from bregma); the contralateral striatum received an equal volume of sterile PBS (vehicle) as the within-animal control. A volume of 2 μL/site of 5 mg/mL PFFs was delivered at 200 nL/min with a 5 min needle dwell to minimize reflux. Brains were collected 1 month post-injection and processed into Triton X-soluble fraction (TSF) and Triton X-insoluble fraction (TIF) by sequential Triton/SDS extraction (see Section 2.4.1), followed by immunoblotting for total αSyn and pS129-αSyn with GAPDH as loading control (see Section 2.4.3). This pilot comprised two animals in total: one *Ide* KO and one *Ide* WT. PFFs preparation and stereotaxic injections were performed with assistance from Weilin Chen and Dr. Pan Gao.

2.4 Protein biochemistry

This section details the methods used for protein extraction, quantification, and analysis, including Western blotting (WB), Bicinchoninic acid (BCA) assay, Thioflavin T (ThT) fluorescence assay, and co-immunoprecipitation (CO-IP).

2.4.1 Protein extraction

For the biochemical separation of soluble and insoluble αSyn species, LUHMES cells and mouse brain tissues were processed using a sequential extraction protocol. Samples were initially lysed in ice-cold Triton Extraction Buffer freshly supplemented with Complete™

Protease Inhibitor Cocktail and PhosSTOP™ Phosphatase Inhibitor Cocktail (Roche). Homogenized lysates were centrifuged at 1,000 × g for 10 minutes at 4 °C to remove nuclei and debris. The supernatant was then subjected to ultracentrifugation at 100,000 × g for 1 hour at 4 °C using 1.5 mL polycarbonate ultracentrifuge tubes (Beckman Coulter). The resulting supernatant was collected as the TSF. The pellet was subsequently resuspended in SDS Extraction Buffer supplemented with the same inhibitor cocktails and thoroughly sonicated in a water bath sonicator (Elma Elmasonic S 10 H, Elma Schmidbauer GmbH, Germany) until the pellet was fully dissolved. This final solution was designated as the TIF.

2.4.2 BCA assay

Total protein concentrations were determined using the Pierce™ BCA Protein Assay Kit (Thermo Fisher Scientific) according to the manufacturer's instructions. The working reagent was prepared by mixing Reagent A and Reagent B at a 50:1 ratio. Samples were incubated with the working solution at 37 °C for 30 minutes. Absorbance was measured at 562 nm using a microplate reader (ClarioStar, BMG labtech, Ortenburg, Germany).

2.4.3 Western blot

Protein concentrations were normalized based on BCA assay results prior to Western blot analysis. Protein samples were mixed with Laemmli sample buffer containing 50 mM DL-dithiothreitol (DTT; Sigma-Aldrich) and denatured by heating at 95 °C for 5 minutes. Equal amounts of protein were separated by SDS-PAGE using 4–20 % Mini-PROTEAN® TGX™ precast protein gels (Bio-Rad Laboratories) in Tris-glycine running buffer. Proteins were transferred onto polyvinylidene difluoride (PVDF) membranes using a Bio-Rad PowerPac™ Basic Power Supply (Bio-Rad Laboratories). Membranes were blocked with 5 % (w/v) bovine serum albumin (BSA; Sigma-Aldrich) in Tris-buffered saline containing 0.1 % (v/v) Tween-20 (TBST) for 1 hour at room temperature. Primary antibodies were diluted in TBST containing

5 % BSA and incubated with the membranes overnight at 4 °C under gentle agitation. After washing, membranes were incubated with appropriate HRP-conjugated secondary antibodies (Cell Signalling Technology) in TBST for 1 hour at room temperature. Protein bands were visualized using the Clarity™ Western ECL Substrate (Bio-Rad Laboratories) and imaged using the ChemiDoc™ MP Imaging System (Bio-Rad Laboratories). Band intensities were quantified using ImageJ software and normalized to the housekeeping protein GAPDH. A list of primary and secondary antibodies used is provided in Appendix C.

2.4.4 ThT fluorescence assay

To assess β-sheet-rich protein aggregates, ThT fluorescence assays were performed on detergent-processed protein samples. Protein concentrations were adjusted to 2 mg/mL using the BCA assay. The Thioflavin T (Sigma-Aldrich) powder was diluted in PBS to a working concentration of 50 µM and filtered through a 0.2 µm syringe filter. For each sample, 50 µL of protein solution was mixed with 50 µL of ThT working solution in a black 96-well clear-bottom plate, yielding a final ThT concentration of 25 µM. Plates were incubated in the dark at room temperature for 30 minutes with gentle shaking. Fluorescence was measured using a microplate reader (ClarioStar, BMG Labtech, Ortenburg, Germany) with excitation and emission wavelengths set to 450 nm and 482 nm, respectively. Buffer-only controls containing detergent and inhibitor mixtures were included for background correction. All conditions were measured in technical duplicates.

2.4.5 Co-immunoprecipitation (Co-IP)

Co-IP was performed using the Pierce™ Crosslink Magnetic IP/Co-IP Kit (Thermo Fisher Scientific) according to the manufacturer's protocol with minor modifications. LUHMES cells were transduced under four conditions: no virus (control), αSyn AV only, EGFP-tagged IDE AV only, or both αSyn and EGFP-tagged IDE AV. An additional group served as a negative

control, in which cells were co-transduced with both AVs, but non-specific rabbit IgG was used instead of the anti-IDE antibody during bead preparation. For each condition, total protein lysates were prepared in IP Lysis/Wash Buffer supplemented with Protease Inhibitor Cocktail (Sigma-Aldrich) and pre-cleared by centrifugation at 13,000 × g for 10 minutes at 4 °C. Input lysates were collected from the same pre-cleared samples prior to incubation with beads and used to assess transduction efficiency and protein expression. To prepare antibody-crosslinked beads, 50 µL of Protein A/G magnetic beads were washed twice with 1× Modified Coupling Buffer and incubated overnight at 4 °C with 200 µL of antibody solution containing 20 µg of anti-IDE antibody (Abcam). On the following day, the beads were washed and crosslinked using 0.25 mM DSS for 30 min at room temperature with gentle mixing. Residual antibody and crosslinker were removed by sequential washes with Elution Buffer and IP Lysis/Wash Buffer. In the negative control group (**Figure 13, rightmost lane**), the beads were incubated with normal rabbit IgG (isotype control) instead of the specific primary antibody, followed by identical processing steps. For immunoprecipitation, 500 µL of pre-cleared lysates were incubated with the crosslinked beads for 1 hour at room temperature under gentle rotation. After binding, the beads were washed twice with IP Lysis/Wash Buffer and once with ultrapure water. Bound protein complexes were eluted using 100 µL of Elution Buffer and immediately neutralized with 13 µL of Neutralization Buffer. Eluted samples and corresponding input lysates were analyzed by SDS-PAGE and immunoblotting as described in Section 2.3.3 using antibodies against IDE, αSyn, and GAPDH.

2.5 Structural modeling and visualization

The interaction between IDE and αSyn was explored using structural prediction and visualization tools. AlphaFold 3 was used to model the IDE–αSyn complex, and PyMOL was applied to analyze hydrogen bonds at the protein–protein interface.

2.5.1 Structural prediction using AlphaFold 3

Structural modeling of the IDE–αSyn complex was performed using AlphaFold 3 on the AlphaFoldServer platform (https://alphafoldserver.com/). Full-length amino acid sequences of human IDE (UniProt: P14735) and αSyn (UniProt: P37840) were submitted in FASTA format. The prediction was performed using default parameters for protein–protein complex modeling. The resulting structure was downloaded in CIF format for further analysis.

2.5.2 Visualization and hydrogen bond analysis

The predicted IDE–αSyn complex was visualized and analyzed using PyMOL (v3.1.1, Schrödinger, LLC). CIF files were imported and displayed in cartoon and stick representation to examine overall structure and interfacial interactions. Hydrogen bonds at the protein–protein interface were identified using PyMOL, applying a donor–acceptor distance threshold of 2.0–3.5 Å. A total of 65 hydrogen bonds were detected and classified based on interatomic distance into the following categories: Ultra Strong (≤2.5 Å), Strong (2.5–3.0 Å), Moderate (3.0–3.2 Å), Weak (3.2–3.5 Å), and Non-effective (>3.5 Å). Hydrogen bonds were visualized as dashed yellow lines, and relevant interacting residues were labeled. The distribution of hydrogen bond categories was summarized using GraphPad Prism and presented in **Figure 12b**.

2.6 Statistical analysis

All statistical analyses were performed using GraphPad Prism version 10.0.2 (GraphPad Software, Inc.). For comparisons between two groups, unpaired two-tailed t-tests were applied. For experiments involving more than two groups, one-way analysis of variance (ANOVA) was conducted, followed by Tukey's multiple comparisons test to determine intergroup differences. Prior to performing ANOVA, homogeneity of variances was verified using Brown–Forsythe and Bartlett's tests. A p-value < 0.05 was considered statistically significant. All data are presented as mean ± SEM, and the number of independent experiments (n) is indicated in the figure legends.

3. Results

3.1 IDE knockdown promotes a shift of endogenous αSyn to the insoluble fraction

To determine whether IDE regulates the solubility of endogenous αSyn, LUHMES cells were transfected with either control or IDE-specific siRNA and subjected to biochemical fractionation into TSF and TIF. Western blot analysis revealed a significant reduction of αSyn in the TSF and a corresponding accumulation in the TIF following IDE knockdown (**Figure 6a**). Densitometric quantification confirmed these changes ($p = 0.0118$ for TSF, $p = 0.0158$ for TIF; **Figure 6b**). GAPDH levels were consistent across samples, confirming equivalent protein loading. IDE knockdown was validated by reduced IDE protein expression. These findings suggest that IDE contributes to the maintenance of αSyn solubility under physiological conditions, and its depletion promotes the transition of αSyn toward an insoluble, potentially aggregation-prone state.

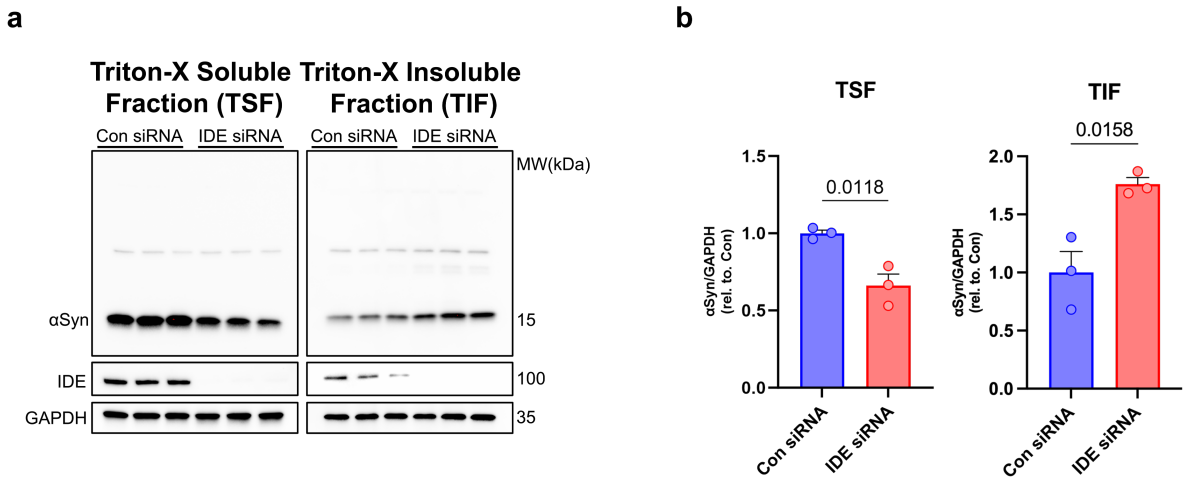

Figure 6. IDE knockdown shifts αSyn solubility in LUHMES cells.

(**a**) Western blot analysis of αSyn in TSF and TIF from LUHMES cells transfected with control or IDE siRNA. IDE knockdown was confirmed by reduced IDE protein levels. GAPDH was used as a loading control. (**b**)

Quantification of αSyn levels normalized to GAPDH and expressed relative to control. Data are mean ± SEM (n = 3). Unpaired two-tailed t-test.

3.2 IDE overexpression does not significantly alter the solubility of endogenous αSyn

To evaluate whether elevating IDE levels modulates endogenous αSyn solubility, LUHMES cells were transduced with IDE-overexpressing AV or left untreated. Cells were fractionated into TSF and TIF fractions and analyzed by Western blot. IDE overexpression effectively elevated IDE protein levels but did not lead to significant changes in αSyn levels in either the TSF or TIF (**Figure 7a**). Quantification supported these findings (p = 0.8934 for TSF, p = 0.1766 for TIF; **Figure 7b**). These results suggest that endogenous IDE may already operate near a functional threshold for αSyn regulation, or that overexpressed IDE cannot effectively access aggregation-prone αSyn under basal conditions without additional stressors that promote misfolding.

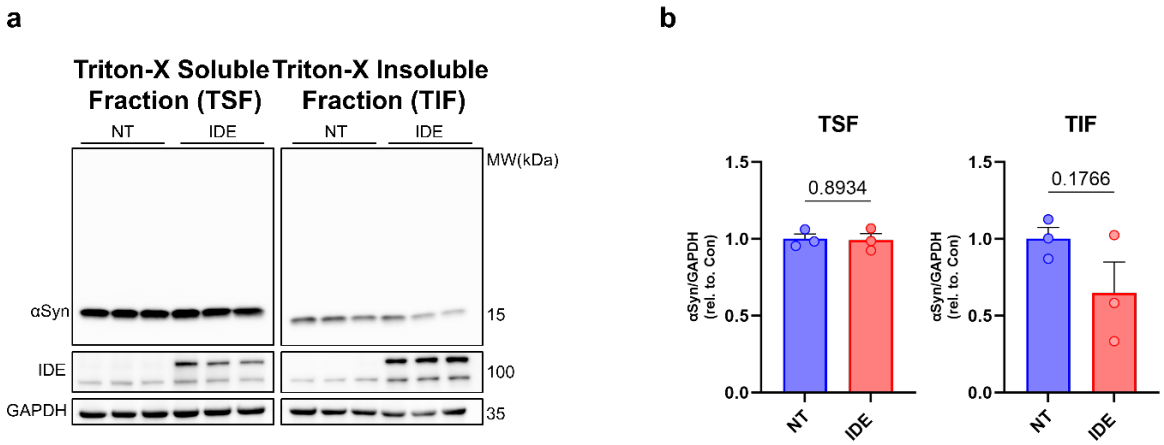

Figure 7. IDE overexpression does not alter the solubility distribution of endogenous αSyn.

(**a**) Western blot analysis of αSyn in TSF and TIF fractions from LUHMES cells transduced with IDE-overexpressing AV or left untreated. GAPDH was used as a loading control. (**b**) Quantification of αSyn levels normalized to GAPDH and expressed relative to the no-treatment group. Data are mean ± SEM (n = 3). Unpaired two-tailed t-test.

3.3 IDE knockdown does not affect *SNCA* transcription but promotes β-sheet aggregate formation

To determine whether the increase in insoluble αSyn observed upon IDE knockdown was due to altered gene expression, we first measured *SNCA* mRNA levels using ddPCR. As shown in **Figure 8a**, *IDE* transcript levels were significantly reduced following siRNA transfection (p < 0.0001), confirming effective knockdown. However, *SNCA* mRNA expression remained unchanged (p = 0.8934), suggesting that IDE does not regulate αSyn at the transcriptional level.

We next examined whether IDE knockdown promotes protein aggregation by performing a ThT assay, which detects β-sheet-rich structures commonly associated with misfolded proteins. As shown in **Figure 8b**, IDE knockdown significantly increased ThT fluorescence intensity (p = 0.0003), indicating an overall accumulation of β-sheet-containing protein aggregates. Although the ThT assay is not specific for αSyn, these results are consistent with our earlier findings of increased insoluble αSyn in the TIF fraction and support the idea that IDE may limit the formation of β-sheet-rich aggregates.

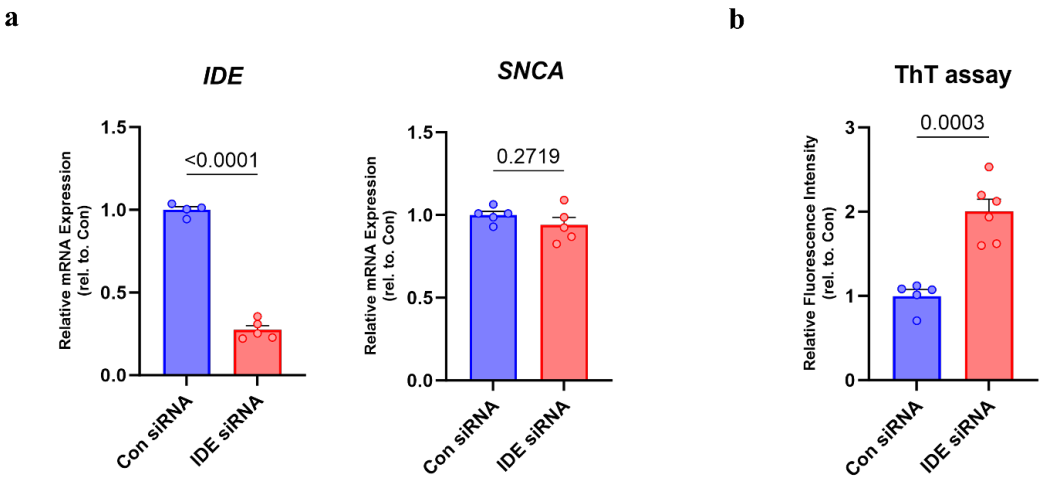

Figure 8. IDE knockdown does not affect *SNCA* transcription but increases β-sheet aggregates.

(**a**) ddPCR analysis of *IDE* and *SNCA* mRNA in LUHMES cells. IDE mRNA was significantly reduced by siRNA, while *SNCA* mRNA showed no change. (**b**) ThT fluorescence assay showing increased β-sheet signal after IDE knockdown. Data are mean ± SEM ($n \geq 4$). Unpaired two-tailed *t*-test.

3.4 IDE modulates αSyn solubility in a pathological overexpression model

To investigate the role of IDE in regulating αSyn solubility under conditions of pathological overexpression, LUHMES cells were transduced with αSyn-overexpressing AV to model elevated αSyn burden. IDE expression was either knocked down using siRNA or upregulated via IDE AV (EGFP-tagged IDE). Following transduction, cells were fractionated into TSF and TIF to assess the distribution of αSyn (**Figure 9a**). In these blots, overexpressed EGFP-tagged IDE appeared as a slower-migrating band at ~140 kDa, whereas endogenous IDE migrated at ~110 kDa, consistent with the mass shift introduced by the GFP tag.

Western blot analysis revealed a significant increase in both TSF and TIF αSyn levels following αSyn overexpression compared to control. Quantification showed that IDE knockdown further increased insoluble αSyn in the TIF ($p < 0.05$), while IDE overexpression significantly reduced

it ($p < 0.01$) (**Figure 9b**). No significant changes were observed in the TSF across IDE-modulated groups ($p > 0.05$).

These data indicate that IDE specifically modulates the aggregation state of αSyn by reducing the accumulation of insoluble αSyn, without affecting its soluble pool. The bidirectional effect of IDE on insoluble αSyn suggests that IDE overexpression mitigates αSyn aggregation, while IDE knockdown exacerbates it, particularly in the context of pathological αSyn overexpression.

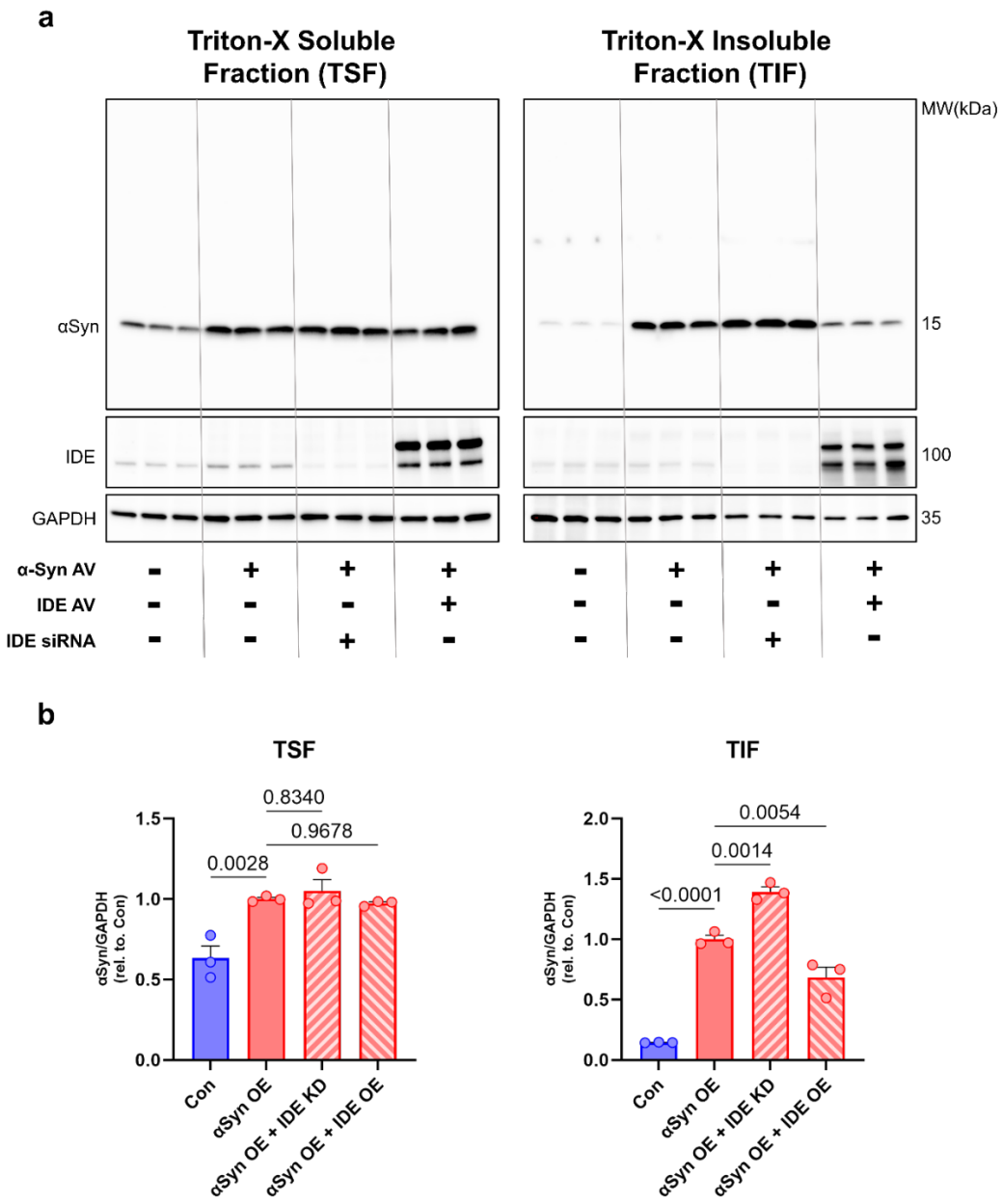

Figure 9. IDE modulation affects overexpressed αSyn solubility.

(a) Western blot of αSyn in TSF and TIF fractions from LUHMES cells with αSyn overexpression, IDE knockdown, or IDE overexpression. Overexpressed EGFP-tagged IDE appears as a slower-migrating band at ~140 kDa, whereas endogenous IDE migrates at ~110 kDa, reflecting the GFP tag. (**b**) Quantification of αSyn levels in TSF and TIF fractions. IDE knockdown increased αSyn in TIF, while IDE overexpression decreased it. Data are presented as mean ± SEM (n = 3). Statistical significance was determined using one-way ANOVA followed by Tukey's multiple comparisons test, with individual p-values indicated in the figure.

3.5 IDE knockdown enhances αSyn induced cytotoxicity in LUHMES cells

To investigate whether IDE modulates αSyn-induced cytotoxicity, LDH release assays were performed in LUHMES cells under different experimental conditions (**Figure 10**).

Initially, to assess the basal cytotoxicity associated with IDE depletion, LUHMES cells were treated with IDE siRNA or control siRNA. Compared to untreated control cells, the control siRNA-treated group exhibited a mild, non-significant increase in LDH release ($p = 0.0577$), suggesting a baseline cytotoxic effect due to the transfection procedure. In contrast, IDE knockdown significantly increased LDH release compared to both untreated controls ($p = 0.0003$) and control siRNA-treated cells ($p = 0.0437$), indicating that IDE depletion specifically exacerbates cell damage independent of transfection-related effects (**Figure 10a**).

Next, to examine the direct impact of protein overexpression, LUHMES cells were separately transduced with viral vectors expressing GFP (as a control protein), IDE, or αSyn (**Figure 10b**). All conditions significantly increased LDH release compared to untreated controls, suggesting general cytotoxic stress induced by viral transduction ($p = 0.0050$, $p = 0.0041$, and $p < 0.0001$, respectively). Notably, αSyn overexpression induced the highest cytotoxicity, consistent with its known pathological role.

Further experiments aimed to evaluate how IDE knockdown influences αSyn-driven toxicity. LUHMES cells co-treated with IDE siRNA and αSyn displayed significantly higher cytotoxicity compared to cells expressing αSyn alone ($p = 0.0027$; **Figure 10c**). This result strongly suggests that IDE depletion exacerbates αSyn-induced cellular injury. Conversely, co-overexpression of IDE and αSyn did not significantly alter cytotoxicity compared to αSyn alone ($p = 0.9367$; **Figure 10d**), indicating that under these conditions, IDE overexpression does not effectively mitigate αSyn-induced damage.

Taken together, these findings support the hypothesis that endogenous IDE is protective against αSyn-induced cytotoxicity in LUHMES cells, particularly highlighting that IDE deficiency significantly aggravates neuronal vulnerability under pathological αSyn conditions.

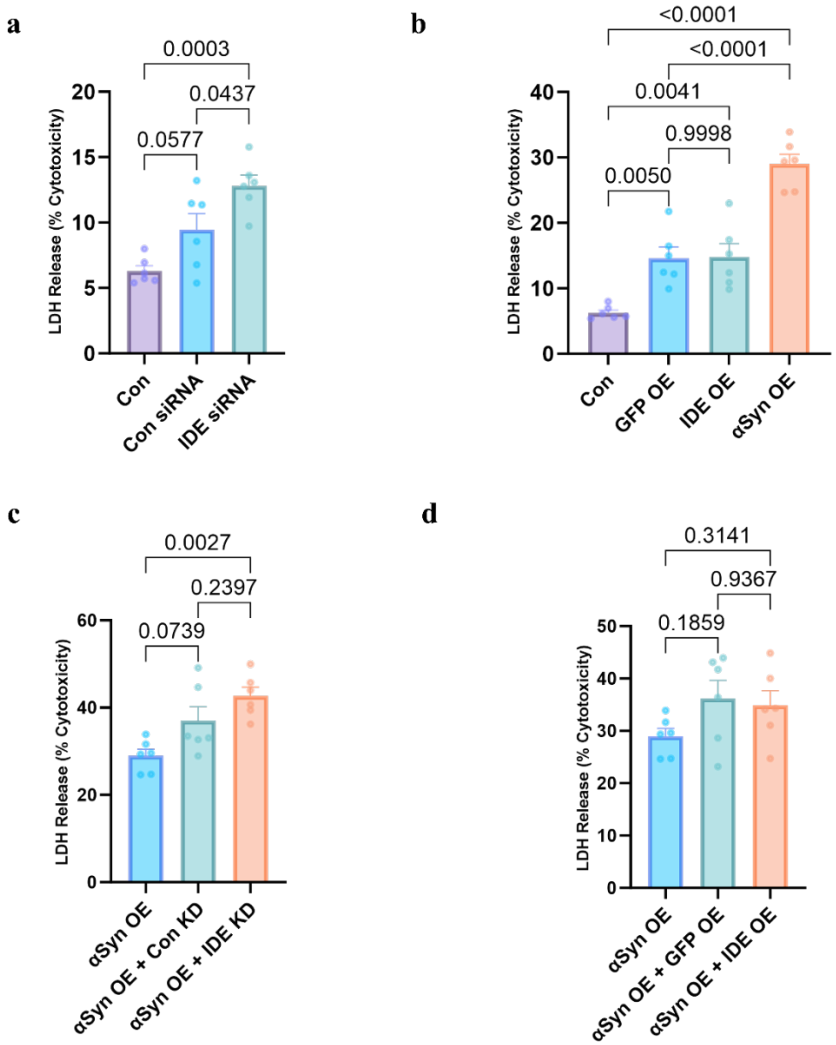

Figure 10. IDE knockdown aggravates αSyn-induced cytotoxicity in LUHMES cells as measured by LDH release.

(**a**) IDE knockdown (IDE siRNA) significantly increased LDH release compared to untreated control cells (Con), while control siRNA induced only mild cytotoxicity. (**b**) Transduction of LUHMES cells with GFP, IDE, or αSyn viral vectors increased cytotoxicity relative to untreated controls, with αSyn overexpression eliciting the strongest cytotoxic response. (**c**) Combined αSyn overexpression and IDE knockdown (IDE KD) resulted in significantly elevated LDH release compared to αSyn alone, whereas the combination with control siRNA (Con KD) showed

no significant difference. (**d**) Co-overexpression of IDE and αSyn did not significantly change cytotoxicity compared to αSyn overexpression alone. Data are presented as mean ± SEM (n = 6). Statistical significance was determined using one-way ANOVA followed by Tukey's multiple comparisons test, with individual p-values indicated in the figure.

3.6 IDE deletion exacerbates αSyn pathology in vivo

At 1 month after unilateral striatal PFFs (with the contralateral striatum injected with PBS as the within-animal control), brains were fractionated into TSF and TIF and analysed by immunoblotting (**Figure 11**). In TIF, pS129-αSyn was higher in the PFFs-injected KO hemisphere than in the PFFs-injected WT hemisphere and than in the PBS-injected side of the same KO animal. Total αSyn in TIF did not clearly increase at this time point. In TSF, the bands for total αSyn and pS129-αSyn looked similar across hemispheres and genotypes, with no obvious changes. IDE loss/presence (KO/WT) and comparable loading (GAPDH) were verified on the same membranes. For completeness, AAV-αSyn was also attempted in the same experiment; no clear trend was observed, and it is therefore not discussed further. This in vivo dataset is a pilot (n = 1 per genotype; single time point) based on whole-hemisphere homogenates; results are presented descriptively without statistical inference, and additional biological replicates and time-course analyses will be required to confirm reproducibility.

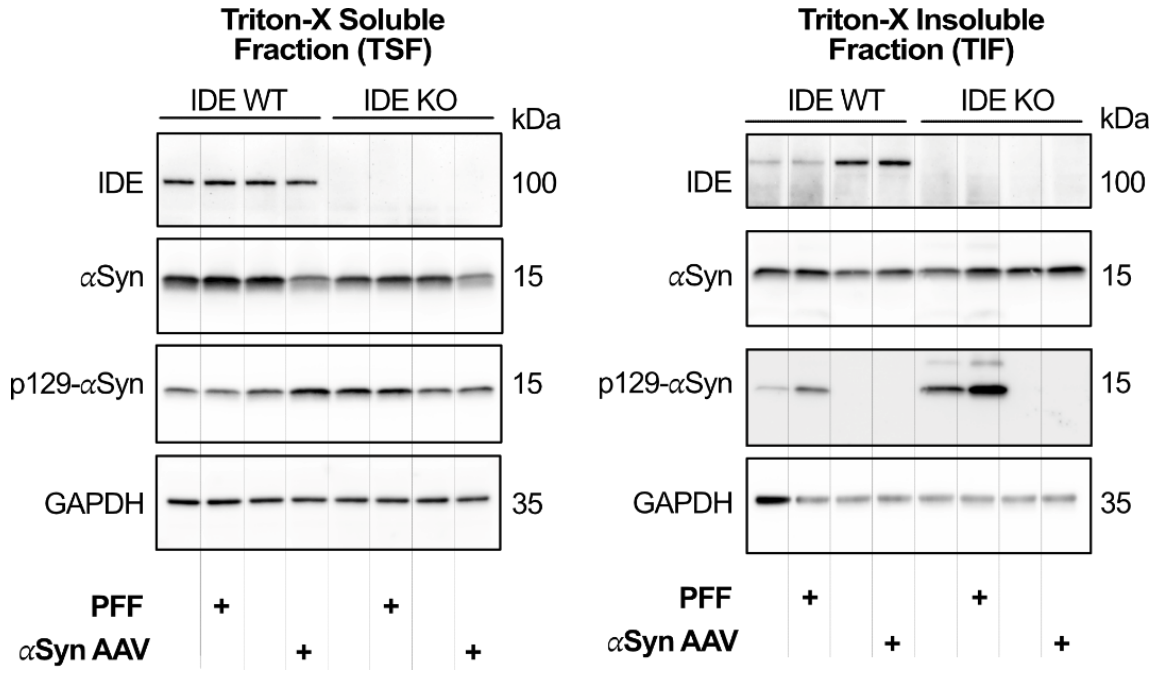

Figure 11. IDE deletion enhances αSyn pathology in vivo.

Western blot analysis of αSyn and pS129-αSyn in the TSF and TIF from *Ide* WT and KO mice following αSyn PFFs or αSyn AAV injection. *Ide* KO mice showed higher levels of pS129-αSyn and total αSyn in the TIF fraction compared to WT. No changes were observed in the TSF fraction. GAPDH was used as a loading control. These observations are based on a single biological replicate, and further validation is required.

3.7 IDE and αSyn interaction predicted by AlphaFold 3

To explore the interaction between IDE and αSyn, we used AlphaFold 3 to predict their binding and subsequently reconstructed the complex using PyMOL. The model indicates that IDE and αSyn form a stable complex, with hydrogen bonds (depicted in yellow) playing a significant role in their interaction. The PyMOL visualization (**Figure 12a**) shows the detailed binding site, highlighting the residues involved in these interactions. The zoomed-in view of the IDE-αSyn binding site further reveals several strong hydrogen bonds between specific residues, indicating a strong and stable binding interface. The hydrogen bond analysis of the IDE-αSyn

complex categorizes the bond strength into ultra-strong (≤2.5 Å), strong (2.5 - 3.0 Å), moderate (3.0 - 3.2 Å), weak (3.2 - 3.5 Å), and no effective interaction (>3.5 Å) (**Figure 12b**). More than 50% of the hydrogen bonds fall within the ultra-strong and strong categories, suggesting that the IDE-αSyn interaction is primarily stabilized by these strong bonds, with a minor contribution from weaker interactions.

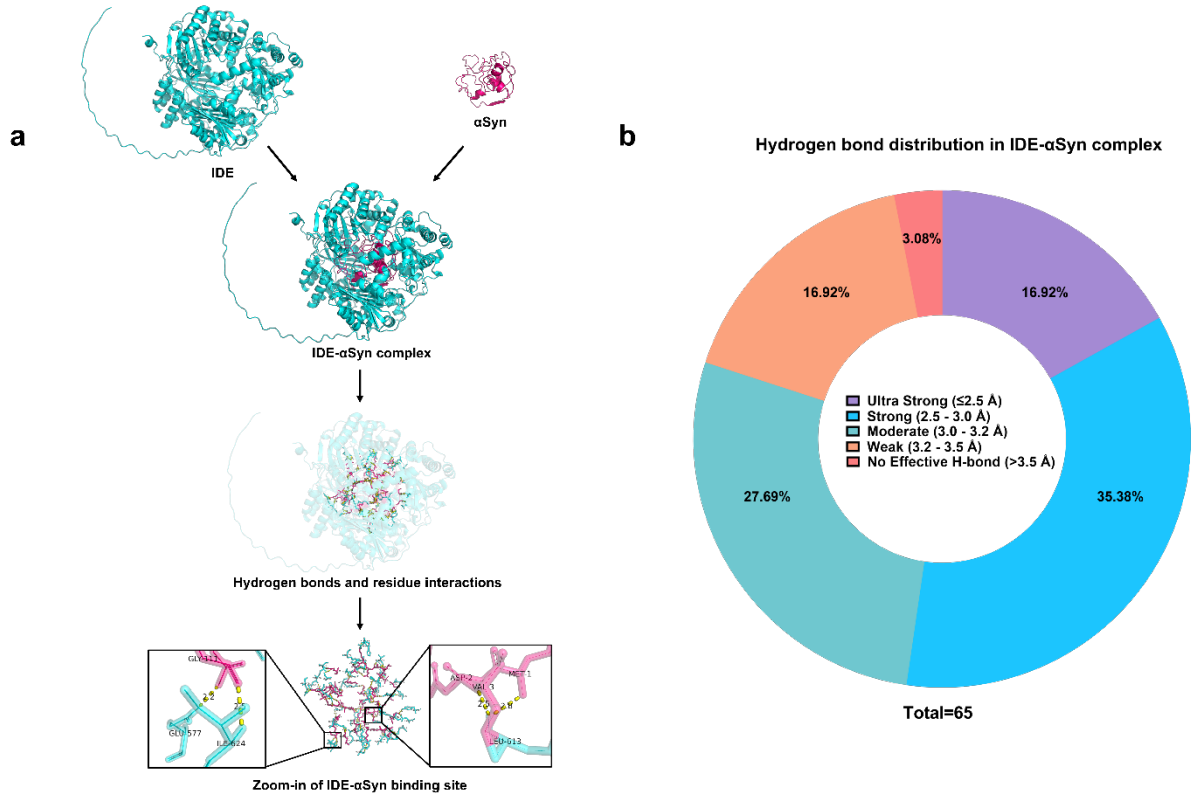

Figure 12. IDE and αSyn interaction predicted by AlphaFold 3 and hydrogen bond distribution.

(**a**) The model shows the interaction between IDE (cyan) and αSyn (magenta). The IDE-αSyn complex is further visualized, highlighting hydrogen bonds (yellow) and residue interactions. The zoom-in view shows detailed interactions at the IDE-αSyn binding site. (**b**) Hydrogen bond distribution in the IDE-αSyn complex, with bond strength categorized as Ultra Strong (≤2.5 Å), Strong (2.5 - 3.0 Å), Moderate (3.0 - 3.2 Å), Weak (3.2 - 3.5 Å), and No Effective H-bond (>3.5 Å). Total bonds = 65.

3.8 Co-IP Reveals IDE and αSyn Interaction

We assessed whether IDE physically associates with αSyn by Co-IP using an anti-IDE antibody in LUHMES cells transduced under four conditions: no virus, αSyn AV only, IDE AV only, or both αSyn and IDE AV. In input lysates, endogenous IDE migrated at ~110 kDa, whereas the overexpressed EGFP-tagged IDE appeared as a slower band at ~140 kDa, consistent with the tag. In IDE Co-IP eluates, αSyn was undetectable without IDE overexpression but was readily recovered when IDE was overexpressed. An IgG control showed no IDE or αSyn signal. These data demonstrate specific recovery of αSyn in IDE pulldowns and support a direct IDE–αSyn interaction, consistent with the structural interaction model.

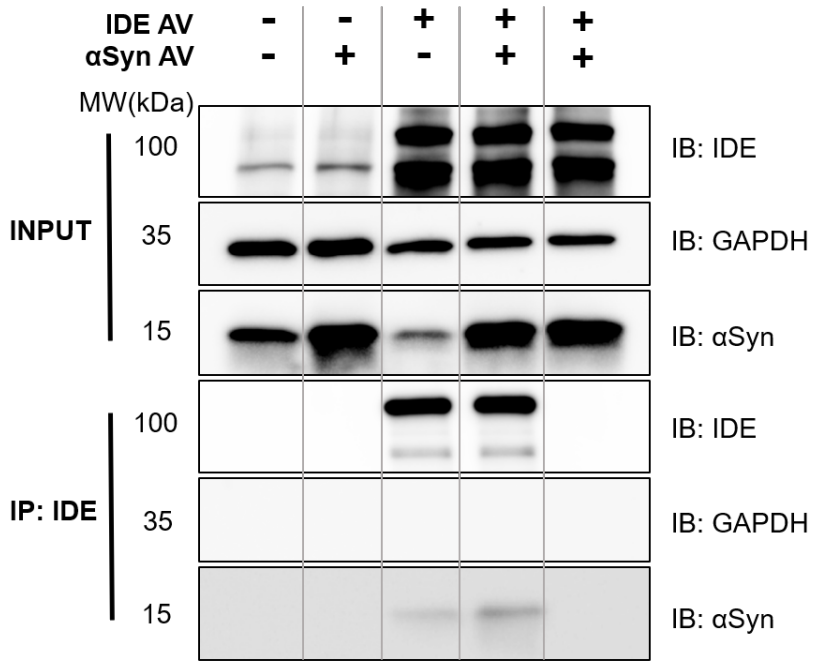

Figure 13. Co-IP of IDE and αSyn in LUHMES Cells.

LUHMES cells were transduced with IDE and αSyn AV, and CO-IP was performed using an anti-IDE antibody. The membrane was probed with an antibody against αSyn, revealing a distinct band around 15 kDa following IDE pulldown, indicating an interaction between IDE and αSyn, overexpressed IDE is EGFP-tagged and migrates at ~140 kDa. The rightmost lane represents the IgG negative control (no IDE antibody during IP). GAPDH serves

as a loading and separation control for input versus IP and is not used for quantitation. Representative data from three independent experiments.

4. Discussion

4.1 IDE modulation alters αSyn aggregation in neuronal models

Knockdown of IDE led to a marked increase in αSyn within the TIF, indicative of enhanced aggregation into detergent-insoluble species (**Figure 6**). This was accompanied by a reduction in αSyn levels in the TSF, consistent with a redistribution of αSyn from soluble to aggregated forms. Collectively, these findings support a regulatory role of IDE in αSyn proteostasis, potentially constraining its conversion toward insoluble aggregates.

To further explore the directionality of this effect, we examined the consequences of IDE overexpression in two experimental contexts. When αSyn was overexpressed to mimic the pathological burden seen in PD, increased IDE levels significantly reduced αSyn partitioning into the insoluble fraction, without major changes in soluble αSyn levels (**Figure 9**). This result mirrors the protective role of IDE observed in knockdown conditions and indicates that IDE acts on aggregation-prone αSyn species rather than globally affecting total protein expression.

However, when IDE was overexpressed in the absence of αSyn overexpression (i.e., under endogenous αSyn conditions), the shift in αSyn distribution appeared less pronounced (**Figure 7**). In contrast to the bidirectional effect seen with IDE knockdown—where reduced IDE levels led to simultaneous increase in TIF and decrease in TSF—IDE overexpression did not cause a reciprocal reduction of endogenous αSyn in the TIF with a concurrent rise in TSF. This asymmetry suggests that the endogenous αSyn pool may be more resistant to modulation, possibly due to lower basal aggregation propensity or ceiling effects in available soluble αSyn (84–87). These findings imply that IDE's capacity to influence αSyn solubility is more pronounced under pathological or aggregation-prone conditions, reinforcing the notion that

IDE primarily targets intermediate or misfolded species that arise during stress or αSyn overproduction.

One interpretation is that IDE interacts with oligomeric or partially misfolded αSyn conformers and facilitates their clearance or sequestration. This model is supported by prior in vitro data from Sharma et al., who showed that substoichiometric concentrations of IDE can hold αSyn oligomers and inhibit fibril elongation (72). In our cellular system, loss of IDE likely removes this buffering interaction, allowing oligomers to coalesce into larger detergent-insoluble aggregates. Conversely, increased IDE may provide protective binding capacity, especially under conditions of αSyn overabundance, thereby preserving αSyn in a more soluble and less toxic state.

Importantly, the lack of significant reduction in soluble αSyn with IDE overexpression supports the idea that IDE does not function as a protease that degrades αSyn monomers. Structural constraints—such as the 140 amino acid length of αSyn—likely preclude efficient access to IDE's catalytic chamber (22,67). Instead, IDE may act in a chaperone-like manner (67,88), transiently binding aggregation-prone intermediates, preventing further misfolding or aggregation, and possibly facilitating delivery to downstream clearance mechanisms.

It is important to contextualize our cell-based results with previous studies and consider alternative explanations. One alternative hypothesis could be that IDE knockdown indirectly affects αSyn aggregation by altering other cellular pathways (for instance, insulin signalling or other proteases) (73,89,90). IDE is known to degrade insulin; however, in our neuronal cultures, insulin levels are externally controlled (culture media) and short-term IDE knockdown is unlikely to induce major insulin signalling changes that would affect αSyn. Another possibility is that IDE knockdown could overload other degradation systems (like the proteasome or lysosomes) by failing to degrade its normal substrates, thereby indirectly reducing αSyn

clearance. While we cannot fully rule out complex indirect effects, the simplest interpretation remains that IDE is acting on αSyn itself, given the strong biochemical evidence for a direct interaction and the specificity of changes in the aggregated fraction. Our CO-IP data (discussed in Section 4.3) directly confirmed that IDE and αSyn associate in the cellular context, lending further credence to a direct mechanism.

Our cell model results are consistent with observations from a non-neuronal system – pancreatic islet β-cells – where IDE deficiency also led to accumulation of αSyn. In *Ide* KO mice, β-cells showed reduced autophagy and increased αSyn levels, suggesting that IDE loss impairs the clearance of αSyn or promotes its aggregation even outside the brain (75). The agreement between the islet data and our neuronal data indicates a conserved role for IDE in managing αSyn levels across cell types. One intriguing aspect from the islet study was that IDE knockdown reduced autophagic flux in β-cells (75). Although we did not directly measure autophagy markers in our main experiments, preliminary data from pilot studies indicated no significant changes in autophagy markers upon IDE knockdown. This observation suggests that the impact of IDE loss on αSyn aggregation may not be directly mediated through alterations in macroautophagy activity. Instead, IDE's interaction with αSyn could influence aggregate formation and clearance independently of overall autophagy flux. For instance, IDE might normally facilitate delivery of αSyn oligomers to lysosomes by preventing their assembly into larger, less digestible aggregates (91–94). Without IDE, aggregates may become excessively large or structurally resistant to efficient autophagic clearance, resembling other pathological scenarios in PD where impaired clearance contributes to a progressive accumulation of αSyn (65,95,96).

In conclusion, our cellular findings provide strong evidence that IDE is an upstream modulator of αSyn aggregation. By reducing IDE levels, cells accumulate more αSyn aggregates, whereas

increasing IDE levels holds aggregation in check. This establishes a causal link between IDE function and αSyn homeostasis in neurons. From a therapeutic standpoint, this result is promising: it implies that augmenting IDE function in neurons might mitigate αSyn aggregation, a key pathology of PD. However, cell culture models have limitations, and it was critical to validate these findings in an organismal context, where the complexity of brain environment and long-term effects come into play. We therefore extended our investigation to in vivo models, as discussed next.

4.2 Loss of IDE exacerbates αSyn pathology in vivo

Under a unilateral striatal PFFs inoculation with the contralateral PBS hemisphere as the within-animal control, biochemical fractionation (TSF/TIF) and immunoblotting were performed at 1-month post-surgery (**Figure 11**). Overall, genotype-dependent differences were largely confined to the insoluble fraction: the *Ide* KO injected hemisphere showed an enhanced pS129-αSyn signal in TIF, whereas total αSyn in TIF did not show a clear increase at this time point; in TSF, total αSyn and pS129-αSyn appeared broadly similar. In view of the limited sample size and time window (n = 1 per genotype; single time point), these observations are presented descriptively without statistical inference. For completeness, AAV-αSyn overexpression was also attempted in the same batch; no consistent trend was observed at 1 month and it is not further elaborated.

Pathologically, PFFs inoculation drives endogenous α-synuclein toward aggregates via a seeding–templating process. pS129-αSyn is widely regarded as a robust molecular hallmark of Lewy-type pathology and is more frequently associated with insoluble/aggregate-related species rather than the soluble pool (97–100). Within seeding paradigms, S129

phosphorylation and aggregate mass accumulation are related but separable, and their time courses need not be synchronous: prior work indicates that pS129 often emerges after the initial deposition and, in some contexts, can attenuate subsequent seeded fibrillization and toxicity (101,102). Consistent with this view, at an early window (1 month) we prioritized TIF-pS129 as the primary readout and focused the comparison on WT-PFFs versus KO-PFFs (with each animal's PBS hemisphere as the within-animal baseline). This strategy is more sensitive for positioning the impact of IDE loss on the enrichment/maturation of pathological α-syn species than relying on TIF-total αSyn or TSF indices at this stage. At the same time, pS129 reflects lesion state/stage rather than toxicity per se (103,104); functional inferences should integrate total levels, soluble/insoluble distribution, and morphology-based assessments (105,106).

Methodological considerations also account for the present readouts. Whole-hemisphere homogenization facilitates comparison within a unified technical framework but may dilute focal lesions; the employed fractionation is inherently more sensitive to insoluble species, making TIF more likely than TSF to show early seeding-related changes, while TSF may remain near baseline at this stage. Moreover, one month lies in the early seeding–amplification phase, and a stabilized rise in TIF total αSyn may not yet be apparent. These factors together underlie the asymmetric signals between TIF and TSF, consistent with the concept that PFFs recruit soluble endogenous α-syn into insoluble Lewy-like inclusions (99,107).

Methodological extensions and validation. Building on the present fractionation/readout framework, related validation has been initiated and is being advanced in independent projects along three axes: (i) expanding sample size with multi-time-point tracking to resolve the temporal relationship between TIF total αSyn and pS129; (ii) conducting regional, quantitative IHC at injection sites and connected nuclei to cross-validate biochemical fractionation; and (iii) adding harsher solubilization for orthogonal confirmation and incorporating functional

readouts where appropriate. These steps lie beyond the scope of this thesis and are therefore not detailed here.

Taken together, under PFFs-induced seeding, loss of IDE is associated with a greater burden of insoluble, pS129-modified α-syn species, directionally concordant with our cellular observations. Given the constraints of sample size and time window, the conclusions remain preliminary; a time course and region-resolved orthogonal validation within the same fractionation framework will help clarify the temporal relationships among pS129, total α-syn levels, and soluble/insoluble distribution, and more firmly link molecular pathology to functional outcomes.

4.3 Direct interaction between IDE and αSyn: validation of a mechanistic link

A central question in this research was how IDE influences αSyn aggregation. Our hypothesis posited a direct interaction between the two proteins, which could allow IDE to "shield" αSyn from aggregating. To test this, we first employed AlphaFold3 structural modelling (108), which predicted a plausible binding interface between IDE and αSyn. The model supported the formation of a stable complex, stabilized by multiple hydrogen bonds and close inter-residue contacts (**Figure 12**). These in silico findings provided a strong rationale to experimentally assess whether such an interaction occurs in cells.

We next performed Co-IP experiments in LUHMES cells to validate this prediction (**Figure 13**). When we overexpressed human IDE and αSyn in the same cells and immunoprecipitated IDE, we were able to detect αSyn in the IDE immunoprecipitate by Western blot, whereas αSyn was not detected in the IgG control immunoprecipitation (rightmost lane), indicating that non-

specific binding was negligible. This result supports a specific physical association between IDE and αSyn in a cellular context.

αSyn was co-precipitated only under IDE overexpression, likely because endogenous IDE levels are too low for detection. The interaction is specific, as αSyn was not pulled down by IgG control or in the absence of IDE. Although biochemical and structural modeling supports an IDE–αSyn interaction, Co-IP detection was only successful upon IDE overexpression, likely due to the transient, low-abundance nature of the interaction and the limited sensitivity of available IDE antibodies.

These technical limitations may partly be explained by structural and biochemical features of IDE. As a large zinc metalloprotease (~110 kDa), IDE adopts a clamshell-like tertiary structure that may shield many of its immunogenic epitopes, particularly in the native state or even partially denatured conditions (70,109). Additionally, the conformational flexibility and domain architecture of IDE may render key epitopes less accessible, especially in the context of folded or aggregated protein complexes. These structural characteristics, together with the inherently low basal expression of IDE in neuronal cells, likely underlie the challenges in achieving consistent and robust immunodetection using currently available commercial antibodies. Taken together, our data suggest that the IDE–αSyn interaction may be biologically transient and low in abundance, but also that its experimental detection is significantly hindered by the limited sensitivity of currently available antibodies. These methodological limitations underscore the need for improved IDE antibody development.

On whether IDE proteolytically degrades α-synuclein. Multiple lines of evidence argue against a proteolytic mechanism (72). First, IDE overexpression reduced TIF-associated αSyn without lowering total or TSF αSyn, whereas IDE deficiency showed the opposite directionality in cells and in vivo, indicating a redistribution between soluble and insoluble pools rather than bulk

degradation. Second, prior in-vitro studies demonstrated that IDE binds αSyn oligomers and blocks fibril elongation in a non-proteolytic manner, with the αSyn C-terminus activating IDE—consistent with a dead-end chaperone/holdase role rather than monomer cleavage (22,72). Third, from a structural standpoint, full-length αSyn (140 aa) is unlikely to efficiently access IDE's catalytic chamber, further arguing against direct proteolysis (110,111). Together with our interaction assays and modeling, these data support a model in which IDE binds and stabilizes/traffics aggregation-prone intermediates, thereby limiting their conversion into insoluble assemblies rather than degrading αSyn monomers. We cannot exclude that IDE may secondarily clear short αSyn-derived peptides generated by other proteases; targeted peptidomics would be required to test this. This non-proteolytic, holdase-like model also anticipates greater vulnerability upon IDE loss, consistent with our subsequent cytotoxicity findings.

Another interesting point is the allosteric activation of IDE by αSyn oligomers reported in vitro. While we did not directly measure IDE's enzymatic activity in our cell or mouse experiments, one might speculate that in PD brains with lots of αSyn aggregates, IDE's activity against its other substrates (like insulin or Aβ) could be modulated by αSyn binding. Sharma et al. saw increased IDE catalytic function on a peptide in the presence of αSyn oligomers (72), presumably via αSyn binding to IDE's exosite. In a living brain, if αSyn binds IDE, it could potentially upregulate IDE's proteolysis of Aβ or other peptides – a fascinating cross-talk between PD and AD pathologies. Alternatively, if too much αSyn binds, it might titrate IDE away from other roles (a paradox highlighted by Leissring (112): what prevents IDE from getting clogged by substrates?) These considerations, though beyond our current data, underscore that the IDE–αSyn interplay might have broader consequences for cell biology than just αSyn aggregation.

From a methodological perspective, confirming the direct interaction lends credibility to our interpretation that the phenotypic effects (more aggregates, more toxicity) are indeed due to IDE's interaction with αSyn, rather than indirect effects. It essentially ties the molecular mechanism to the phenotype. This kind of validation is crucial in complex diseases: many modifiers might affect aggregation indirectly (e.g., via signalling pathways), but showing a physical interaction often indicates a primary mechanism. In conclusion, we have verified that IDE and αSyn physically interact. This interaction provides a mechanistic explanation for IDE's ability to modulate αSyn aggregation: IDE can directly bind αSyn, influencing its aggregation pathway. By confirming this, we strengthen the argument for IDE being a direct "anti-aggregation" factor for αSyn. This mechanistic insight is vital if we consider therapeutic targeting – for instance, any drug that enhances IDE's binding to αSyn (or stabilizes the IDE–αSyn complex) could mimic the effect of IDE overexpression, potentially reducing aggregation. Conversely, if some conditions reduce IDE–αSyn binding affinity (like certain mutations or post-translational modifications), those could increase aggregation and be targets to avoid. Having covered the interaction and aggregation aspects, we next consider how these molecular events translate into cellular consequences, namely cytotoxicity, and what that means for the disease process.

4.4 Impact of IDE on αSyn induced cytotoxicity

The ultimate relevance of modulating αSyn aggregation is its effect on neuronal survival and toxicity. Our study addressed this by examining how IDE levels influence αSyn–mediated cytotoxicity in neuronal cultures. We employed the LDH release assay as an indicator of cell membrane damage and death. The results revealed a clear pattern: IDE knockdown increased cell vulnerability to αSyn toxicity, whereas IDE overexpression did not significantly reduce

toxicity under the conditions tested (**Figure 10**). Several specific observations support this conclusion. First, we found that knocking down IDE alone (in the absence of any αSyn overexpression) caused a modest but significant increase in LDH release compared to untreated control cells (**Figure 10a**), indicating that loss of IDE makes neurons more susceptible to stress or baseline damage. This was a meaningful result – it suggests IDE has an intrinsic cytoprotective role even without exogenous αSyn challenges, possibly by clearing endogenous toxic peptides or maintaining proteostasis. Notably, even cells treated with a non-targeting control siRNA showed a slight rise in LDH (relative to untreated), likely due to transfection stress, but the IDE siRNA effect was above that baseline. This hints that IDE depletion predisposes neurons to damage, consistent with the idea that IDE is a housekeeping enzyme that, when removed, leads to accumulation of cytotoxic peptides (which could include αSyn or others) (72,73,78).

Second, when we introduced αSyn overexpression via a viral vector in cells, we observed the expected increase in toxicity – αSyn overexpressing cells released substantially more LDH than controls (**Figure 10b**), reflecting αSyn's known toxic effects when accumulated (113,114). Importantly, in cells that combined αSyn overexpression with IDE knockdown, the toxicity was exacerbated beyond that seen with αSyn alone. This synergistic worsening (IDE loss + αSyn) strongly suggests that IDE normally mitigates αSyn's toxic potential, and removing it unleashes greater injury. Quantitatively, co-treatment of cells with αSyn overexpression and IDE siRNA led to a significant increase in LDH release ($p = 0.0027$ in our data) compared to αSyn overexpression with control siRNA (**Figure 10c**). In contrast, cells that had αSyn overexpression plus IDE overexpression did not show a statistically significant reduction in LDH relative to αSyn alone. In fact, αSyn + IDE-overexp had similar LDH levels as αSyn-only, indicating that simply adding more IDE did not rescue viability ($p = 0.93$, no difference;

Figure 10d). This outcome might seem initially disappointing, but it provides important insights into the dynamics of proteostasis and toxicity.

The finding that IDE knockdown aggravates αSyn toxicity is very much in line with our aggregation results and supports the hypothesis that aggregated or oligomeric αSyn is the toxic species. By knocking down IDE, we saw more aggregates (Section 4.1) and accordingly more cell death here. This dovetails with the widely held view that αSyn oligomers/fibrils are what kill neurons (26,115). With less IDE, more toxic oligomers likely accumulate and damage cells, perhaps by permeabilizing membranes or disrupting essential processes. It is also consistent with other studies where impairing protein clearance leads to heightened toxicity of aggregation-prone proteins. For instance, inhibiting autophagy in αSyn transgenic mice worsened neurodegeneration (116–118), and knocking down Hsp70 (a chaperone) increased αSyn toxicity in neuronal cultures (119,120). IDE can now be added to this list of proteostasis components whose loss intensifies proteotoxic stress.

The lack of a rescue effect with IDE overexpression requires some consideration. There are a few possible explanations: (1) The overexpression of αSyn in our model might produce such high levels of αSyn that even additional IDE cannot counteract the toxicity. It could be a threshold effect – IDE may be effective up to a point, but if αSyn burden is extreme, the protective mechanisms are overwhelmed. We did see that IDE overexpression reduced aggregates, but perhaps the remaining aggregates (or soluble oligomers not prevented) were still enough to cause maximal toxicity. In other words, αSyn overexpression might have a ceiling effect on toxicity in this acute model, such that removing IDE makes it even worse, but adding IDE cannot reduce toxicity below the baseline of αSyn alone which might already be near maximal for that system. (2) Another consideration is that while IDE overexpression prevents new aggregates (as we saw), it might not be able to disassemble pre-formed aggregates

or oligomers that are already toxic. If αSyn starts aggregating, adding IDE later may not reverse that damage easily. In contrast, IDE knockdown likely prevents cells from handling even initial oligomers, making everything worse quickly (121–123). (3) It's also possible that IDE overexpression has diminishing returns due to cellular regulation – for example, very high IDE might be inhibited by endogenous IDE regulators or might form inactive homodimers (IDE can form dimers that are less active under some conditions) (110,124). If so, beyond a certain level, extra IDE doesn't equate to extra activity.

Interestingly, we observed that overexpression of IDE alone (without αSyn overexpression) did cause a slight increase in LDH release compared to untreated cells, though this was confounded by the fact that any viral transduction (even a control GFP virus) increased LDH a bit. All virally transduced groups (GFP control, IDE, αSyn) showed more LDH than untreated cells, likely due to general viral vector stress or high protein load. IDE overexpression did not significantly differ from GFP control in toxicity, suggesting IDE itself is not toxic when overexpressed. This is important for potential therapy: raising IDE in neurons doesn't seem to kill them by itself (at least acutely). The mild LDH increase in all vector-treated cells underscores that our assay is sensitive to any perturbation, which is why we compare within those groups.

Combining these observations, the net effect is that endogenous IDE provides a protective baseline (its removal worsens outcomes), but adding more IDE beyond normal does not further protect in the face of strong toxic insults. This asymmetry is not uncommon in biological systems – for many protective factors, loss is detrimental, but gain beyond normal is not proportionately beneficial, due to either saturation or because other steps become limiting (125). It might be that in our system, once IDE is sufficient to handle a certain amount of αSyn, other

factors (like the rate of αSyn production or the presence of other co-factors) become the bottleneck for toxicity.

From a disease perspective, these findings imply that having too little IDE is clearly a risk factor for neuronal damage in the context of high αSyn, while having extra IDE might not easily cure already sick neurons. This could mean that therapeutic strategies might need to focus on preventing loss of IDE function (for example, avoiding conditions that reduce IDE expression or functional competence) rather than relying on late-stage IDE overexpression once pathology is established. Nevertheless, a more nuanced approach to enhance IDE function—for instance by stabilizing the enzyme, facilitating its availability, or selectively promoting its interaction with αSyn—could still be beneficial, but will require careful evaluation in disease-relevant models.

Our results also suggest that IDE knockdown alone caused some damage (higher LDH than control), indicating IDE has substrates or functions beyond αSyn that are important for cell survival. Potentially, the absence of IDE could lead to accumulation of other toxic peptides (maybe amylin, or bradykinin fragments, etc., though neurons don't produce insulin, they might produce other IDE substrates). Or possibly, IDE knockdown causes mild dysregulation of insulin/IGF signalling even in neuron-like cells (IDE can degrade IGF-II, for instance) (112,126). This raises an alert that chronic IDE inhibition (if one were to consider it for some reason) could be harmful to neurons. In contrast, IDE overexpression did not harm cells on its own, which is reassuring.

In summary, our cytotoxicity experiments confirm that IDE serves a neuroprotective function in the face of αSyn stress. The absence of IDE significantly worsens neuron damage caused by αSyn accumulation, supporting the idea that IDE normally mitigates αSyn's toxic effects. This finding is consistent with the increased aggregation observed in those conditions – more

aggregates likely translated into more cell death. While boosting IDE above normal did not rescue cells in our acute model, this does not preclude its potential utility; it suggests that timing and the magnitude of αSyn stress are critical variables. It may be that in a more chronic or progressive model (like a slowly developing transgenic mouse), moderate elevation of IDE could slow the accumulation of pathology and thereby slow neurodegeneration.

We have now discussed how IDE influences αSyn aggregation, pathology, and toxicity. The evidence across these domains converges to a coherent picture: IDE is a protective factor that restrains αSyn aggregation and the resulting neurotoxic consequences, whereas loss of IDE removes this restraint and accelerates pathology. We will now synthesize the broader implications of these findings for PD and outline future directions for research and therapeutic development.

4.5 Implications for PD pathogenesis and therapeutic prospects

The collective findings of my doctoral research highlight IDE as an important modulator of αSyn proteostasis and toxicity, offering several implications for understanding PD pathogenesis.

IDE as a Protective Buffer in αSynopathies: Our data suggest that IDE is part of the neuronal proteostasis network that safeguards against αSyn aggregation. Endogenous IDE appears to provide a buffer such that when αSyn levels rise or misfold (as in PD), IDE may bind the misfolded αSyn species, thereby reducing the likelihood of pathological aggregate formation (**Figure 6**). Only when proteostasis is severely impaired, due to factors such as aging, overwhelming αSyn burden, or genetic influences, do aggregates accumulate substantially (127). This fits a broader theme in neurodegeneration: there is often a long prodromal phase

where cells manage misfolded proteins via chaperones and degradation systems until those systems start failing (23). IDE may be one of the components that becomes insufficient in the aging brain, enabling αSyn to progressively aggregate. It would be interesting to examine IDE levels or activity in post-mortem PD brains across different stages; it is conceivable that brains with advanced αSyn pathology might show reduced IDE function or IDE sequestered into LBs (128,129), potentially diminishing its protective capacity.

Linking Metabolic Disease and Neurodegeneration: Our results strengthen the biological connection between type 2 diabetes/metabolic syndrome and PD. IDE is a known risk locus for T2D, and our work shows that IDE deficiency worsens αSyn pathology (**Figure 9**), suggesting a mechanistic pathway through which metabolic dysfunction may influence PD progression. In insulin-resistant states, IDE may be chronically occupied with degrading excess insulin and islet amyloid polypeptide, reducing its availability to handle αSyn in the brain (75). Consistent with this mechanism, epidemiological studies have noted that patients with diabetes have a higher risk of developing PD and tend to experience more severe symptoms (76,80,130). Compromised IDE function may thus represent a contributing factor linking metabolic dysfunction to neurodegeneration. Supporting this notion, some anti-diabetic drugs, such as GLP-1 receptor agonists that do not burden IDE, have shown neuroprotective effects in PD clinical trials (131,132), whereas insulin secretagogues, which raise insulin levels and could saturate IDE, have not—although this remains speculative (81). These observations underscore the importance of further investigating how systemic metabolic states influence brain proteostasis and αSyn pathology.

IDE and Other Clearance Pathways – Synergy or Redundancy? IDE does not operate in isolation but intersects with other protein clearance mechanisms, particularly the lysosomal system. Our study hints that IDE might help funnel misfolded αSyn towards autophagic

degradation (75). IDE binding could keep αSyn soluble enough to be recognized by CMA or to be efficiently engulfed by macroautophagy. If IDE is absent, αSyn might form aggregates that are poor CMA substrates, clogging lysosomal pathways (43). This suggests that therapies aimed at enhancing autophagy might work more effectively in the presence of robust IDE function, and combination strategies enhancing both IDE function and lysosomal clearance could synergistically reduce αSyn pathology.

Therapeutic Targeting of IDE: From a therapeutic perspective, IDE presents both opportunities and challenges. Being an enzyme, IDE is amenable to pharmacological modulation, and small-molecule activators have been described in the context of diabetes (133,134). Upregulating IDE in the brain could hypothetically reduce αSyn aggregation; however, because IDE also degrades insulin and other peptides, strategies must avoid systemic metabolic disturbances. Ideally, future interventions would selectively enhance IDE's interaction with αSyn without broadly affecting its other substrates.

Biomarker Potential: If IDE levels or IDE function with αSyn pathology, they could serve as biomarkers for disease progression. Measuring IDE or its proteolytic signature in patient samples could provide insights into an individual's proteostatic reserve, encouraging further investigation into IDE as a potential diagnostic or prognostic marker.

Overlap with Alzheimer's and other Proteinopathies: IDE is already well-studied in Alzheimer's for Aβ clearance (73,135), and our findings suggest an overlapping role in PD for αSyn. This raises the intriguing possibility that enhancing IDE might impact multiple aggregation-prone proteins simultaneously. However, competition between substrates could complicate outcomes, particularly in elderly individuals with mixed pathologies, underscoring the need for targeted therapeutic strategies.

Together, these findings not only illuminate IDE's multifaceted role in αSyn proteostasis but also open several promising avenues for future research and therapeutic development. Building on this work, several directions are worth pursuing, including investigating whether enhancing IDE function or stability can slow αSyn aggregation and neurodegeneration in PD models, characterizing the structural interaction between IDE and αSyn to inform therapeutic strategies, and exploring how neuronal stress affects IDE regulation and function. Extending these investigations to other synucleinopathies and the gut–brain axis may further elucidate IDE's broader role in neurodegeneration. While translating these findings to humans will require considerable research, our results provide a proof-of-concept that bolstering intrinsic proteostasis mechanisms—specifically through IDE—could complement approaches aimed at reducing αSyn burden. Harnessing IDE's protective function without perturbing its other roles will be critical, but success in this direction may ultimately enable prediction of individual proteostatic resilience and inform personalized interventions for PD and related disorders. Together, these findings open the door for interdisciplinary strategies targeting the intersection of metabolic regulation and neurodegeneration.

References

1. Berg D, Postuma RB, Bloem B, Chan P, Dubois B, Gasser T, et al. Time to redefine PD? Introductory statement of the MDS Task Force on the definition of Parkinson's disease. Mov Disord. 2014 Apr;29(4):454–62.

2. Wang S, Jiang Y, Yang A, Meng F, Zhang J. The Expanding Burden of Neurodegenerative Diseases: An Unmet Medical and Social Need. Aging and disease. 2024 Nov 9;0.

3. Reeve A, Simcox E, Turnbull D. Ageing and Parkinson's disease: Why is advancing age the biggest risk factor? Ageing Res Rev. 2014 Mar;14(100):19–30.

4. Koeglsperger T, Rumpf SL, Schließer P, Struebing FL, Brendel M, Levin J, et al. Neuropathology of incidental Lewy body & prodromal Parkinson's disease. Mol Neurodegeneration. 2023 May 12;18(1):32.

5. Shin HW, Hong SW, Youn YC. Clinical Aspects of the Differential Diagnosis of Parkinson's Disease and Parkinsonism. J Clin Neurol. 2022 May;18(3):259–70.

6. Simon C, Soga T, Okano HJ, Parhar I. α-Synuclein-mediated neurodegeneration in Dementia with Lewy bodies: the pathobiology of a paradox. Cell Biosci. 2021 Nov 19;11:196.

7. Calabresi P, Mechelli A, Natale G, Volpicelli-Daley L, Di Lazzaro G, Ghiglieri V. Alpha-synuclein in Parkinson's disease and other synucleinopathies: from overt neurodegeneration back to early synaptic dysfunction. Cell Death Dis. 2023 Mar 1;14(3):176.

8. Simon DK, Tanner CM, Brundin P. Parkinson Disease Epidemiology, Pathology, Genetics, and Pathophysiology. Clin Geriatr Med. 2020 Feb;36(1):1–12.

9. Dorsey ER, Sherer T, Okun MS, Bloem BR. The Emerging Evidence of the Parkinson Pandemic. J Parkinsons Dis. 8(Suppl 1):S3–8.

10. Khanna A, Adams J, Antoniades C, Bloem BR, Carroll C, Cedarbaum J, et al. Accelerating Parkinson's Disease drug development with federated learning approaches. npj Parkinsons Dis. 2024 Nov 21;10(1):1–9.

11. Dorsey ER, Elbaz A, Nichols E, Abbasi N, Abd-Allah F, Abdelalim A, et al. Global, regional, and national burden of Parkinson's disease, 1990–2016: a systematic analysis for the Global Burden of Disease Study 2016. The Lancet Neurology. 2018 Nov 1;17(11):939–53.

12. Tanner CM. Advances in environmental epidemiology. Movement Disorders. 2010;25(S1):S58–62.

13. Tran J, Anastacio H, Bardy C. Genetic predispositions of Parkinson's disease revealed in patient-derived brain cells. npj Parkinsons Dis. 2020 Apr 24;6(1):1–18.

14. Nalls MA, Blauwendraat C, Vallerga CL, Heilbron K, Bandres-Ciga S, Chang D, et al. Identification of novel risk loci, causal insights, and heritable risk for Parkinson's disease: a meta-genome wide association study. Lancet Neurol. 2019 Dec;18(12):1091–102.

15. Maroteaux L, Campanelli JT, Scheller RH. Synuclein: a neuron-specific protein localized to the nucleus and presynaptic nerve terminal. J Neurosci. 1988 Aug 1;8(8):2804–15.

16. Burré J, Sharma M, Tsetsenis T, Buchman V, Etherton MR, Südhof TC. α-Synuclein Promotes SNARE-Complex Assembly in Vivo and in Vitro. Science. 2010 Sept 24;329(5999):1663–7.

17. Chen J, Zaer S, Drori P, Zamel J, Joron K, Kalisman N, et al. The structural heterogeneity of α-synuclein is governed by several distinct subpopulations with interconversion times slower than milliseconds. Structure. 2021 Sept 2;29(9):1048-1064.e6.

18. Doherty CPA, Ulamec SM, Maya-Martinez R, Good SC, Makepeace J, Khan GN, et al. A short motif in the N-terminal region of α-synuclein is critical for both aggregation and function. Nat Struct Mol Biol. 2020 Mar;27(3):249–59.

19. Flagmeier P, Meisl G, Vendruscolo M, Knowles TPJ, Dobson CM, Buell AK, et al. Mutations associated with familial Parkinson's disease alter the initiation and

amplification steps of α-synuclein aggregation. Proc Natl Acad Sci U S A. 2016 Sept 13;113(37):10328–33.

20. Kalia LV, Kalia SK, McLean PJ, Lozano AM, Lang AE. α-Synuclein oligomers and clinical implications for Parkinson disease. Ann Neurol. 2013 Feb;73(2):155–69.

21. Vidović M, Rikalovic MG. Alpha-Synuclein Aggregation Pathway in Parkinson's Disease: Current Status and Novel Therapeutic Approaches. Cells. 2022 May 24;11(11):1732.

22. Sharma SK, Chorell E, Wittung-Stafshede P. Insulin-degrading enzyme is activated by the C-terminus of α-synuclein. Biochemical and Biophysical Research Communications. 2015 Oct;466(2):192–5.

23. Lehtonen Š, Sonninen TM, Wojciechowski S, Goldsteins G, Koistinaho J. Dysfunction of Cellular Proteostasis in Parkinson's Disease. Front Neurosci. 2019;13:457.

24. Gao V, Briano JA, Komer LE, Burré J. Functional and Pathological Effects of α-Synuclein on Synaptic SNARE Complexes. J Mol Biol. 2023 Jan 15;435(1):167714.

25. Negi S, Khurana N, Duggal N. The misfolding mystery: α-synuclein and the pathogenesis of Parkinson's disease. Neurochemistry International. 2024 July 1;177:105760.

26. Xu CK, Meisl G, Andrzejewska EA, Krainer G, Dear AJ, Castellana-Cruz M, et al. α-Synuclein oligomers form by secondary nucleation. Nat Commun. 2024 Aug 17;15(1):7083.

27. Musteikytė G, Jayaram AK, Xu CK, Vendruscolo M, Krainer G, Knowles TPJ. Interactions of α-synuclein oligomers with lipid membranes. Biochimica et Biophysica Acta (BBA) - Biomembranes. 2021 Apr 1;1863(4):183536.

28. Emin D, Zhang YP, Lobanova E, Miller A, Li X, Xia Z, et al. Small soluble α-synuclein aggregates are the toxic species in Parkinson's disease. Nat Commun. 2022 Sept 20;13(1):5512.

29. Parra-Rivas LA, Madhivanan K, Aulston BD, Wang L, Prakashchand DD, Boyer NP, et al. Serine-129 phosphorylation of α-synuclein is an activity-dependent trigger for

physiologic protein-protein interactions and synaptic function. Neuron. 2023 Dec 20;111(24):4006-4023.e10.

30. Ray B, Mahalakshmi AM, Tuladhar S, Bhat A, Srinivasan A, Pellegrino C, et al. "Janus-Faced" α-Synuclein: Role in Parkinson's Disease. Front Cell Dev Biol. 2021 May 28;9:673395.

31. Kim S, Kwon SH, Kam TI, Panicker N, Karuppagounder SS, Lee S, et al. Transneuronal Propagation of Pathologic α-Synuclein from the Gut to the Brain Models Parkinson's disease. Neuron. 2019 Aug 21;103(4):627-641.e7.

32. Wu Q, Takano H, Riddle DM, Trojanowski JQ, Coulter DA, Lee VMY. α-Synuclein (αSyn) Preformed Fibrils Induce Endogenous αSyn Aggregation, Compromise Synaptic Activity and Enhance Synapse Loss in Cultured Excitatory Hippocampal Neurons. J Neurosci. 2019 June 26;39(26):5080–94.

33. Xie YX, Naseri NN, Fels J, Kharel P, Na Y, Lane D, et al. Lysosomal exocytosis releases pathogenic α-synuclein species from neurons in synucleinopathy models. Nat Commun. 2022 Aug 22;13(1):4918.

34. Lee HJ, Bae EJ, Lee SJ. Extracellular α--synuclein-a novel and crucial factor in Lewy body diseases. Nat Rev Neurol. 2014 Feb;10(2):92–8.

35. Leak RK, Frosch MP, Beach TG, Halliday GM. α-Synuclein: Prion or Prion-like? Acta Neuropathol. 2019 Oct;138(4):509–14.

36. Kuang Y, Mao H, Huang X, Chen M, Dai W, Gan T, et al. α-Synuclein seeding amplification assays for diagnosing synucleinopathies: an innovative tool in clinical implementation. Translational Neurodegeneration. 2024 Nov 21;13(1):56.

37. Fusco G, Chen SW, Williamson PTF, Cascella R, Perni M, Jarvis JA, et al. Structural basis of membrane disruption and cellular toxicity by α-synuclein oligomers. Science. 2017 Dec 15;358(6369):1440–3.

38. Kuo G, Kumbhar R, Blair W, Dawson VL, Dawson TM, Mao X. Emerging targets of α-synuclein spreading in α-synucleinopathies: a review of mechanistic pathways and interventions. Mol Neurodegener. 2025 Jan 23;20(1):10.

39. Xu L, Pu J. Alpha-Synuclein in Parkinson's Disease: From Pathogenetic Dysfunction to Potential Clinical Application. Parkinsons Dis. 2016;2016:1720621.

40. Poewe W, Seppi K, Tanner CM, Halliday GM, Brundin P, Volkmann J, et al. Parkinson disease. Nat Rev Dis Primers. 2017 Mar 23;3(1):1–21.

41. Ebrahimi-Fakhari D, Wahlster L, McLean PJ. Protein degradation pathways in Parkinson's disease: curse or blessing. Acta Neuropathol. 2012 Aug;124(2):153–72.

42. Xilouri M, Brekk OR, Stefanis L. α-Synuclein and protein degradation systems: a reciprocal relationship. Mol Neurobiol. 2013 Apr;47(2):537–51.

43. Cuervo AM, Stefanis L, Fredenburg R, Lansbury PT, Sulzer D. Impaired degradation of mutant alpha-synuclein by chaperone-mediated autophagy. Science. 2004 Aug 27;305(5688):1292–5.

44. Lowe J, Blanchard A, Morrell K, Lennox G, Reynolds L, Billett M, et al. Ubiquitin is a common factor in intermediate filament inclusion bodies of diverse type in man, including those of Parkinson's disease, Pick's disease, and Alzheimer's disease, as well as Rosenthal fibres in cerebellar astrocytomas, cytoplasmic bodies in muscle, and mallory bodies in alcoholic liver disease. J Pathol. 1988 May;155(1):9–15.

45. McNaught KSP, Mytilineou C, JnoBaptiste R, Yabut J, Shashidharan P, Jenner P, et al. Impairment of the ubiquitin-proteasome system causes dopaminergic cell death and inclusion body formation in ventral mesencephalic cultures. Journal of Neurochemistry. 2002;81(2):301–6.

46. McNaught KSP, Perl DP, Brownell AL, Olanow CW. Systemic exposure to proteasome inhibitors causes a progressive model of Parkinson's disease. Ann Neurol. 2004 July;56(1):149–62.

47. Tetzlaff JE, Putcha P, Outeiro TF, Ivanov A, Berezovska O, Hyman BT, et al. CHIP targets toxic alpha-Synuclein oligomers for degradation. J Biol Chem. 2008 June 27;283(26):17962–8.

48. Dawson TM, Dawson VL. The Role of Parkin in Familial and Sporadic Parkinson's Disease. Mov Disord. 2010;25(0 1):S32–9.

49. Bence NF, Sampat RM, Kopito RR. Impairment of the Ubiquitin-Proteasome System by Protein Aggregation. Science. 2001 May 25;292(5521):1552–5.

50. Mizushima N, Komatsu M. Autophagy: renovation of cells and tissues. Cell. 2011 Nov 11;147(4):728–41.

51. Fleming A, Bourdenx M, Fujimaki M, Karabiyik C, Krause GJ, Lopez A, et al. The different autophagy degradation pathways and neurodegeneration. Neuron. 2022 Mar 16;110(6):935–66.

52. Cuervo AM, Wong E. Chaperone-mediated autophagy: roles in disease and aging. Cell Res. 2014 Jan;24(1):92–104.

53. Martinez-Vicente M, Talloczy Z, Kaushik S, Massey AC, Mazzulli J, Mosharov EV, et al. Dopamine-modified α-synuclein blocks chaperone-mediated autophagy. J Clin Invest. 2008 Feb 1;118(2):777–88.

54. Winslow AR, Chen CW, Corrochano S, Acevedo-Arozena A, Gordon DE, Peden AA, et al. α-Synuclein impairs macroautophagy: implications for Parkinson's disease. J Cell Biol. 2010 Sept 20;190(6):1023–37.

55. Mazzulli JR, Xu YH, Sun Y, Knight AL, McLean PJ, Caldwell GA, et al. Gaucher disease glucocerebrosidase and α-synuclein form a bidirectional pathogenic loop in synucleinopathies. Cell. 2011 July 8;146(1):37–52.

56. Cui H, Norrbacka S, Myöhänen TT. Prolyl oligopeptidase acts as a link between chaperone-mediated autophagy and macroautophagy. Biochemical Pharmacology. 2022 Mar 1;197:114899.

57. Narendra D, Tanaka A, Suen DF, Youle RJ. Parkin is recruited selectively to impaired mitochondria and promotes their autophagy. Journal of Cell Biology. 2008 Nov 24;183(5):795–803.

58. Dehay B, Bové J, Rodríguez-Muela N, Perier C, Recasens A, Boya P, et al. Pathogenic lysosomal depletion in Parkinson's disease. J Neurosci. 2010 Sept 15;30(37):12535–44.

59. Date Y, Sasazawa Y, Kitagawa M, Gejima K, Suzuki A, Saya H, et al. Novel autophagy inducers by accelerating lysosomal clustering against Parkinson's disease. Elife. 2024 July 3;13:e98649.

60. Lee J, Sung KW, Bae EJ, Yoon D, Kim D, Lee JS, et al. Targeted degradation of α-synuclein aggregates in Parkinson's disease using the AUTOTAC technology. Molecular Neurodegeneration. 2023 June 24;18(1):41.

61. Auluck PK, Chan HYE, Trojanowski JQ, Lee VMY, Bonini NM. Chaperone suppression of alpha-synuclein toxicity in a Drosophila model for Parkinson's disease. Science. 2002 Feb 1;295(5556):865–8.

62. Hoozemans JJM, van Haastert ES, Eikelenboom P, de Vos R a. I, Rozemuller JM, Scheper W. Activation of the unfolded protein response in Parkinson's disease. Biochem Biophys Res Commun. 2007 Mar 16;354(3):707–11.

63. Colla E, Coune P, Liu Y, Pletnikova O, Troncoso JC, Iwatsubo T, et al. Endoplasmic Reticulum Stress Is Important for the Manifestations of α-Synucleinopathy In Vivo. J Neurosci. 2012 Mar 7;32(10):3306–20.

64. Vogiatzi T, Xilouri M, Vekrellis K, Stefanis L. Wild type alpha-synuclein is degraded by chaperone-mediated autophagy and macroautophagy in neuronal cells. J Biol Chem. 2008 Aug 29;283(35):23542–56.

65. Webb JL, Ravikumar B, Atkins J, Skepper JN, Rubinsztein DC. Alpha-Synuclein is degraded by both autophagy and the proteasome. J Biol Chem. 2003 July 4;278(27):25009–13.

66. Malagelada C, Jin ZH, Jackson-Lewis V, Przedborski S, Greene LA. Rapamycin protects against neuron death in in vitro and in vivo models of Parkinson's disease. J Neurosci. 2010 Jan 20;30(3):1166–75.

67. Tundo GR, Grasso G, Persico M, Tkachuk O, Bellia F, Bocedi A, et al. The Insulin-Degrading Enzyme from Structure to Allosteric Modulation: New Perspectives for Drug Design. Biomolecules. 2023 Oct 7;13(10):1492.

68. Broh-Kahn RH, Mirsky IA. The inactivation of insulin by tissue extracts; the effect of fasting on the insulinase content of rat liver. Arch Biochem. 1949 Jan;20(1):10–4.

69. Mirsky IA, Broh-Kahn RH. The inactivation of insulin by tissue extracts; the distribution and properties of insulin inactivating extracts. Arch Biochem. 1949 Jan;20(1):1–9.

70. Shen Y, Joachimiak A, Rich Rosner M, Tang WJ. Structures of human insulin-degrading enzyme reveal a new substrate recognition mechanism. Nature. 2006 Oct;443(7113):870–4.

71. Kurochkin IV, Goto S. Alzheimer's beta-amyloid peptide specifically interacts with and is degraded by insulin degrading enzyme. FEBS Lett. 1994 May 23;345(1):33–7.

72. Sharma SK, Chorell E, Steneberg P, Vernersson-Lindahl E, Edlund H, Wittung-Stafshede P. Insulin-degrading enzyme prevents α-synuclein fibril formation in a nonproteolytical manner. Sci Rep. 2015 July 31;5:12531.

73. Farris W, Mansourian S, Chang Y, Lindsley L, Eckman EA, Frosch MP, et al. Insulin-degrading enzyme regulates the levels of insulin, amyloid beta-protein, and the beta-amyloid precursor protein intracellular domain in vivo. Proc Natl Acad Sci U S A. 2003 Apr 1;100(7):4162–7.

74. Leissring MA, Farris W, Chang AY, Walsh DM, Wu X, Sun X, et al. Enhanced proteolysis of beta-amyloid in APP transgenic mice prevents plaque formation, secondary pathology, and premature death. Neuron. 2003 Dec 18;40(6):1087–93.

75. Steneberg P, Bernardo L, Edfalk S, Lundberg L, Backlund F, Östenson CG, et al. The Type 2 Diabetes–Associated Gene Ide Is Required for Insulin Secretion and Suppression of α-Synuclein Levels in β-Cells. Diabetes. 2013 June;62(6):2004–14.

76. Bantounou MA, Shoaib K, Mazzoleni A, Modalavalasa H, Kumar N, Philip S. The association between type 2 diabetes mellitus and Parkinson's disease; a systematic review and meta-analysis. Brain Disorders. 2024 Sept 1;15:100158.

77. Cheong JLY, de Pablo-Fernandez E, Foltynie T, Noyce AJ. The Association Between Type 2 Diabetes Mellitus and Parkinson's Disease. J Parkinsons Dis. 2020;10(3):775–89.

78. Sousa L, Guarda M, Meneses MJ, Macedo MP, Vicente Miranda H. Insulin-degrading enzyme: an ally against metabolic and neurodegenerative diseases. The Journal of Pathology. 2021;255(4):346–61.

79. Aktürk T, Çakır M, Saçmacı H, Caniklioğlu A, Tanık N. Is there a role of insulin degrading enzyme in Parkinson's disease? Neurology Asia. 2022 Oct 1;27(3):689–94.

80. Ribarič S. The Contribution of Type 2 Diabetes to Parkinson's Disease Aetiology. International Journal of Molecular Sciences. 2024 Jan;25(8):4358.

81. Qin X, Zhang X, Li P, Wang M, Yan L, Bao Z, et al. Association Between Diabetes Medications and the Risk of Parkinson's Disease: A Systematic Review and Meta-Analysis. Front Neurol. 2021;12:678649.

82. Scholz D, Pöltl D, Genewsky A, Weng M, Waldmann T, Schildknecht S, et al. Rapid, complete and large-scale generation of post-mitotic neurons from the human LUHMES cell line. J Neurochem. 2011 Dec;119(5):957–71.

83. Tang Q, Gao P, Arzberger T, Höllerhage M, Herms J, Höglinger G, et al. Alpha-Synuclein defects autophagy by impairing SNAP29-mediated autophagosome-lysosome fusion. Cell Death Dis. 2021 Sept 17;12(10):854.

84. Wasim A, Menon S, Mondal J. Modulation of α-synuclein aggregation amid diverse environmental perturbation. Elife. 2024 Aug 1;13:RP95180.

85. Awa S, Suzuki G, Masuda-Suzukake M, Nonaka T, Saito M, Hasegawa M. Phosphorylation of endogenous α-synuclein induced by extracellular seeds initiates at the pre-synaptic region and spreads to the cell body. Sci Rep. 2022 Jan 21;12(1):1163.

86. Vasili E, Dominguez-Meijide A, Flores-León M, Al-Azzani M, Kanellidi A, Melki R, et al. Endogenous Levels of Alpha-Synuclein Modulate Seeding and Aggregation in Cultured Cells. Mol Neurobiol. 2022 Feb;59(2):1273–84.

87. Mahul-Mellier AL, Burtscher J, Maharjan N, Weerens L, Croisier M, Kuttler F, et al. The process of Lewy body formation, rather than simply α-synuclein fibrillization, is one of the major drivers of neurodegeneration. Proceedings of the National Academy of Sciences. 2020 Mar 3;117(9):4971–82.

88. Kurochkin IV, Guarnera E, Berezovsky IN. Insulin-Degrading Enzyme in the Fight against Alzheimer's Disease. Trends Pharmacol Sci. 2018 Jan;39(1):49–58.

89. Abdul-Hay SO, Kang D, McBride M, Li L, Zhao J, Leissring MA. Deletion of insulin-degrading enzyme elicits antipodal, age-dependent effects on glucose and insulin tolerance. PLoS One. 2011;6(6):e20818.

90. Marotta NP, Lee VMY. Modelling the Cellular Fate of alpha-Synuclein Aggregates: a Pathway to Pathology. Curr Opin Neurobiol. 2022 Feb;72:171–7.

91. Lee HJ, Khoshaghideh F, Patel S, Lee SJ. Clearance of α-Synuclein Oligomeric Intermediates via the Lysosomal Degradation Pathway. J Neurosci. 2004 Feb 25;24(8):1888–96.

92. Wildburger NC, Hartke AS, Schidlitzki A, Richter F. Current Evidence for a Bidirectional Loop Between the Lysosome and Alpha-Synuclein Proteoforms. Front Cell Dev Biol. 2020;8:598446.

93. Kakuda K, Ikenaka K, Kuma A, Doi J, Aguirre C, Wang N, et al. Lysophagy protects against propagation of α-synuclein aggregation through ruptured lysosomal vesicles. Proc Natl Acad Sci U S A. 2024 Jan 2;121(1):e2312306120.

94. Drobny A, Boros FA, Balta D, Prieto Huarcaya S, Caylioglu D, Qazi N, et al. Reciprocal effects of alpha-synuclein aggregation and lysosomal homeostasis in synucleinopathy models. Transl Neurodegener. 2023 June 13;12(1):31.

95. Lopes da Fonseca T, Villar-Piqué A, Outeiro TF. The Interplay between Alpha-Synuclein Clearance and Spreading. Biomolecules. 2015 Apr 14;5(2):435–71.

96. Yang F, Yang Y ping, Mao C jie, Liu L, Zheng H fen, Hu L fang, et al. Crosstalk between the proteasome system and autophagy in the clearance of α-synuclein. Acta Pharmacol Sin. 2013 May;34(5):674–80.

97. Fujiwara H, Hasegawa M, Dohmae N, Kawashima A, Masliah E, Goldberg MS, et al. alpha-Synuclein is phosphorylated in synucleinopathy lesions. Nat Cell Biol. 2002 Feb;4(2):160–4.

98. Volpicelli-Daley LA, Luk KC, Lee VMY. Addition of exogenous α-synuclein preformed fibrils to primary neuronal cultures to seed recruitment of endogenous α-synuclein to Lewy body and Lewy neurite–like aggregates. Nat Protoc. 2014 Sept;9(9):2135–46.

99. Luk KC, Kehm V, Carroll J, Zhang B, O'Brien P, Trojanowski JQ, et al. Pathological α-synuclein transmission initiates Parkinson-like neurodegeneration in nontransgenic mice. Science. 2012 Nov 16;338(6109):949–53.

100. Henrich MT, Geibl FF, Lakshminarasimhan H, Stegmann A, Giasson BI, Mao X, et al. Determinants of seeding and spreading of α-synuclein pathology in the brain. Sci Adv. 2020 Nov;6(46):eabc2487.

101. Ghanem SS, Majbour NK, Vaikath NN, Ardah MT, Erskine D, Jensen NM, et al. α-Synuclein phosphorylation at serine 129 occurs after initial protein deposition and inhibits seeded fibril formation and toxicity. Proc Natl Acad Sci U S A. 2022 Apr 12;119(15):e2109617119.

102. Ramalingam N, Jin SX, Moors TE, Fonseca-Ornelas L, Shimanaka K, Lei S, et al. Dynamic physiological α-synuclein S129 phosphorylation is driven by neuronal activity. npj Parkinsons Dis. 2023 Jan 16;9(1):4.

103. Lashuel HA, Mahul-Mellier AL, Novello S, Hegde RN, Jasiqi Y, Altay MF, et al. Revisiting the specificity and ability of phospho-S129 antibodies to capture alpha-synuclein biochemical and pathological diversity. npj Parkinsons Dis. 2022 Oct 20;8(1):1–19.

104. Stewart T, Sossi V, Aasly JO, Wszolek ZK, Uitti RJ, Hasegawa K, et al. Phosphorylated α-synuclein in Parkinson's disease: correlation depends on disease severity. Acta Neuropathol Commun. 2015 Jan 31;3:7.

105. Magalhães P, Lashuel HA. Opportunities and challenges of alpha-synuclein as a potential biomarker for Parkinson's disease and other synucleinopathies. NPJ Parkinsons Dis. 2022 July 22;8(1):93.

106. Gallegos S, Pacheco C, Peters C, Opazo CM, Aguayo LG. Features of alpha-synuclein that could explain the progression and irreversibility of Parkinson's disease. Front Neurosci. 2015;9:59.

107. Volpicelli-Daley LA, Luk KC, Patel TP, Tanik SA, Riddle DM, Stieber A, et al. Exogenous α-synuclein fibrils induce Lewy body pathology leading to synaptic dysfunction and neuron death. Neuron. 2011 Oct 6;72(1):57–71.

108. Abramson J, Adler J, Dunger J, Evans R, Green T, Pritzel A, et al. Addendum: Accurate structure prediction of biomolecular interactions with AlphaFold 3. Nature. 2024 Dec;636(8042):E4.

109. Tundo GR, Grasso G, Persico M, Tkachuk O, Bellia F, Bocedi A, et al. The Insulin-Degrading Enzyme from Structure to Allosteric Modulation: New Perspectives for Drug Design. Biomolecules. 2023 Oct 7;13(10):1492.

110. Hulse RE, Ralat LA, Tang WJ. Structure, Function, and Regulation of Insulin-Degrading Enzyme. Vitam Horm. 2009;80:635–48.

111. Mancl JM, Liang WG, Bayhi NL, Wei H, Budell W, Mendez JH, et al. Characterization and modulation of human insulin degrading enzyme conformational dynamics to control enzyme activity. bioRxiv. 2025 Sept 11;2024.12.30.630732.

112. Leissring MA. Insulin-Degrading Enzyme: Paradoxes and Possibilities. Cells. 2021 Sept 16;10(9):2445.

113. Höllerhage M, Moebius C, Melms J, Chiu WH, Goebel JN, Chakroun T, et al. Protective efficacy of phosphodiesterase-1 inhibition against alpha-synuclein toxicity revealed by compound screening in LUHMES cells. Sci Rep. 2017 Sept 13;7(1):11469.

114. Hornung S, Vogl DP, Naltsas D, Volta BD, Ballmann M, Marcon B, et al. Multi-Targeting Macrocyclic Peptides as Nanomolar Inhibitors of Self- and Cross-Seeded Amyloid Self-Assembly of α-Synuclein. Angew Chem Int Ed Engl. 2025 Apr 1;64(14):e202422834.

115. Yoo JM, Lin Y, Heo Y, Lee YH. Polymorphism in alpha-synuclein oligomers and its implications in toxicity under disease conditions. Front Mol Biosci. 2022;9:959425.

116. Choi I, Zhang Y, Seegobin SP, Pruvost M, Wang Q, Purtell K, et al. Microglia clear neuron-released α-synuclein via selective autophagy and prevent neurodegeneration. Nat Commun. 2020 Mar 13;11(1):1386.

117. Choi I, Heaton GR, Lee YK, Yue Z. Regulation of α-synuclein homeostasis and inflammasome activation by microglial autophagy. Sci Adv. 2022 Oct 28;8(43):eabn1298.

118. Tu HY, Yuan BS, Hou XO, Zhang XJ, Pei CS, Ma YT, et al. α-synuclein suppresses microglial autophagy and promotes neurodegeneration in a mouse model of Parkinson's disease. Aging Cell. 2021 Dec;20(12):e13522.

119. Klucken J, Shin Y, Masliah E, Hyman BT, McLean PJ. Hsp70 Reduces alpha-Synuclein Aggregation and Toxicity. J Biol Chem. 2004 June 11;279(24):25497–502.

120. Jones DR, Moussaud S, McLean P. Targeting heat shock proteins to modulate α-synuclein toxicity. Ther Adv Neurol Disord. 2014 Jan;7(1):33–51.

121. Murray KA, Hu CJ, Pan H, Lu J, Abskharon R, Bowler JT, et al. Small molecules disaggregate alpha-synuclein and prevent seeding from patient brain-derived fibrils. Proc Natl Acad Sci U S A. 2023 Feb 14;120(7):e2217835120.

122. Bengoa-Vergniory N, Roberts RF, Wade-Martins R, Alegre-Abarrategui J. Alpha-synuclein oligomers: a new hope. Acta Neuropathol. 2017 Dec;134(6):819–38.

123. Sharma SK, Priya S. Expanding role of molecular chaperones in regulating α-synuclein misfolding; implications in Parkinson's disease. Cell Mol Life Sci. 2017 Feb;74(4):617–29.

124. Song ES, Rodgers DW, Hersh LB. A monomeric variant of insulin degrading enzyme (IDE) loses its regulatory properties. PLoS One. 2010 Mar 16;5(3):e9719.

125. Kafri R, Levy M, Pilpel Y. The regulatory utilization of genetic redundancy through responsive backup circuits. Proc Natl Acad Sci U S A. 2006 Aug 1;103(31):11653–8.

126. Guo Q, Manolopoulou M, Bian Y, Schilling AB, Tang WJ. Molecular basis for the recognition and cleavages of IGF-II, TGF-α, and amylin by human insulin degrading enzyme. J Mol Biol. 2010 Jan 15;395(2):430.

127. Han D, Zheng W, Wang X, Chen Z. Proteostasis of α-Synuclein and Its Role in the Pathogenesis of Parkinson's Disease. Front Cell Neurosci. 2020;14:45.

128. Kalia LV, Lang AE. Parkinson's disease. Lancet. 2015 Aug 29;386(9996):896–912.

129. Wakabayashi K, Tanji K, Mori F, Takahashi H. The Lewy body in Parkinson's disease: molecules implicated in the formation and degradation of alpha-synuclein aggregates. Neuropathology. 2007 Oct;27(5):494–506.

130. Han K, Kim B, Lee SH, Kim MK. A nationwide cohort study on diabetes severity and risk of Parkinson disease. NPJ Parkinsons Dis. 2023 Jan 27;9:11.

131. Meissner WG, Remy P, Giordana C, Maltête D, Derkinderen P, Houéto JL, et al. Trial of Lixisenatide in Early Parkinson's Disease. N Engl J Med. 2024 Apr 4;390(13):1176–85.

132. Athauda D, Maclagan K, Skene SS, Bajwa-Joseph M, Letchford D, Chowdhury K, et al. Exenatide once weekly versus placebo in Parkinson's disease: a randomised, double-blind, placebo-controlled trial. Lancet. 2017 Oct 7;390(10103):1664–75.

133. Tang WJ. Targeting insulin-degrading enzyme to treat type 2 diabetes. Trends Endocrinol Metab. 2016 Jan;27(1):24–34.

134. Cabrol C, Huzarska MA, Dinolfo C, Rodriguez MC, Reinstatler L, Ni J, et al. Small-molecule activators of insulin-degrading enzyme discovered through high-throughput compound screening. PLoS One. 2009;4(4):e5274.

135. Qiu WQ, Walsh DM, Ye Z, Vekrellis K, Zhang J, Podlisny MB, et al. Insulin-degrading enzyme regulates extracellular levels of amyloid beta-protein by degradation. J Biol Chem. 1998 Dec 4;273(49):32730–8.

Appendix A: Cell Culture Materials and Reagents

Material	Cat. Num.	Supplier
Thermo Scientific™ Nunc™ EasYFlask™ Cell Culture Flasks		Thermo Fisher Scientific
Nunc EasYFlask 75cm²	10364131	
Nunc EasYFlask 25cm²	12034917	
Thermo Scientific™ Nunc™ Cell-Culture Treated Multidishes		
6-Well Cell Culture Dish	10119831	Thermo Fisher Scientific
12-Well Cell Culture Dish	10098870	
24-Well Cell Culture Dish	10604903	
48-Well Cell Culture Dish	10644901	
Greiner Bio-One CELLSTAR 96-well, Cell Culture-Treated, Flat-Bottom Microplate	07-000-135	Greiner
Stericup Quick Release-GP Sterile Vacuum Filtration System		Millipore
Stericup-GP 250mL	S2GPU02RE	
Stericup-GP 500mL	S2GPU05RE	
Poly-L-ornithine solution	P4957	Sigma-Aldrich
Human Fibronectin Protein, CF	1918-FN	R&D Systems
Dulbecco's Modified Eagle's Medium/Nutrient Mixture F-12 Ham (DMEM/F-12)	D8062	Sigma-Aldrich

N-2 Supplement (100X)	17502048	Thermo Fisher Scientific
Recombinant Human FGF-basic (154 a.a.)	100-18B	PeproTech
Tetracycline hydrochloride	T7660	Sigma-Aldrich
Recombinant Human GDNF Protein	212-GD-010	Bio-Techne
N6,2′-O-Dibutyryladenosine 3′,5′-cyclic monophosphate sodium salt (Dibutyryl cyclic-AMP)	D0627	Sigma-Aldrich
Dulbecco's phosphate-buffered saline (DPBS), no calcium, no magnesium	14190169	Thermo Fisher Scientific
Trypsin-EDTA solution	T3924	Sigma-Aldrich
Trypan Blue solution	T8154	Sigma-Aldrich
Fetal Bovine Serum (FBS/FCS)	F9665	Sigma-Aldrich
Silencer™ Select predefined siRNA (Gene symbol:IDE; SiRNA ID: s7117)	4392422	Thermo Fisher Scientific
Silencer™ Negative Control No. 1 siRNA	AM4611	Invitrogen™
Opti-MEM™ I Reduced Serum Medium	31985062	Gibco™
Lipofectamine™ RNAiMAX Transfection Reagent	13778150	Invitrogen™

Appendix B: Biochemical Assays Reagents and Instruments

Reagent / Instrument (Full Name)	Abbreviation / Assay ID	Cat. Num.	Supplier
RNeasy Mini Kit	—	74104	Qiagen
QuantiTect Reverse Transcription Kit	—	205311	Qiagen
Qubit 3 Fluorometer	—	Q33226	Thermo Fisher Scientific
Qubit RNA HS Assay Kit	—	Q32852	Thermo Fisher Scientific
TaqMan Gene Expression Assay (*IDE*)	Hs00610452_m1	4448892	Thermo Fisher Scientific
TaqMan Gene Expression Assay (*SNCA*)	Hs00240906_m1	4453320	Thermo Fisher Scientific
ddPCR Supermix for Probes (no dUTP)	—	1863024	Bio-Rad
QX200 Droplet Digital PCR System	—	1864001	Bio-Rad
QX200 Droplet Generator	—	1864002	Bio-Rad
DG8 Cartridges and Gaskets	—	1864008	Bio-Rad

Droplet Generation Oil for Probes	—	1863005	Bio-Rad
C1000 Touch Thermal Cycler	—	1851197	Bio-Rad
PX1 PCR Plate Sealer	—	1814000	Bio-Rad
ChemiDoc MP Imaging System	—	12003154	Bio-Rad
Clarity Western ECL Substrate	—	1705060	Bio-Rad
Mini-PROTEAN TGX Precast Protein Gel (4–20%)	—	4561094	Bio-Rad
Laemmli Sample Buffer	—	1610747	Bio-Rad
Methanol, 99%	—	L13255.0F	Thermo Scientific
DL-Dithiothreitol	DTT	43815	Sigma-Aldrich
PVDF Membranes	—	IPVH00010	Merck Millipore
Bovine Serum Albumin	BSA	A7030	Sigma-Aldrich
Tween-20	—	P1379	Sigma-Aldrich
Triton X-100	—	T9284	Sigma-Aldrich
Sodium dodecyl sulfate solution	20% SDS	05030	Sigma-Aldrich
Thioflavin T	ThT	T3516	Sigma-Aldrich

Protease Inhibitor Cocktail	—	P8340	Sigma-Aldrich
Phosphatase Inhibitor Cocktail 2	—	P5726	Sigma-Aldrich
Restore™ PLUS Western Blot Stripping Buffer	—	46430	Thermo Fisher Scientific
ROTI®Histofix	PFA	A146.1	Carl ROTH
Pierce™ BCA Protein Assay Kits	—	23227	Thermo Fisher Scientific
CytoTox-ONE™ Homogeneous Membrane Integrity Assay	—	G7890	Promega
CLARIOstar Plus plate reader	Plate reader	—	BMG LABTECH
1.5 mL, Microfuge Microcentrifuge Polypropylene Tubes with Snap-On Caps	—	356090	Beckman Coulter
Pierce™ Crosslink Magnetic IP/Co-IP Kit	—	88805	Thermo Fisher Scientific

Appendix C: Antibody List

Antibody	Cat. Num.	Application	Dilution	Supplier
IDE Antibody (F-9), Mouse monoclonal	sc-393887	WB	1:250	Santa Cruz Biotechnology
Anti-Insulin degrading enzyme	ab228720	WB	1:500	Abcam
Anti-Insulin degrading enzyme	ab228720	CO-IP	1:100	Abcam
Mouse Anti-α-Synuclein (42/α-Synuclein)	610787	WB	1:1000	BD Biosciences
Anti-Alpha-synuclein antibody [MJFR1], Rabbit	ab138501	WB	1:1000	Abcam
Anti-Alpha-synuclein (phospho S129) antibody [EP1536Y]	ab51253	WB	1:1000	Abcam
Alpha Synuclein Recombinant Rabbit Monoclonal Antibody (14H2L1)	701085	WB	1:2000	Invitrogen
GAPDH Monoclonal antibody (1E6D9)	60004-1-Ig	WB	1:2500	Proteintech

β-Actin (8H10D10) Mouse mAb	3700	WB	1:1000	Cell Signaling
Anti-rabbit IgG, HRP-linked Antibody	7074	WB	1:5000	Cell Signaling Technology
Anti-mouse IgG, HRP-linked Antibody	7076	WB	1:5000	Cell Signaling Technology

Appendix D: Extraction Buffers and Electrophoresis Solutions

buffer	Reagent	Final conc.	Amount
1% Triton Base Buffer	Triton X-100	1%	0.5 mL
	5 M NaCl	150 mM	1.5 mL
	1 M HEPES pH 7.4	20 mM	1 mL
	0.5 M EDTA	1 mM	100 µL
	1 M $MgCl_2$	1.5 mM	75 µL
	100% glycerol	10%	5 mL
	Milli-Q H_2O	n/a	41.825 mL
	Total		50 mL
Triton Extraction Buffer	1% Triton Base Buffer	—	4.9 mL
	Protease Inhibitor Cocktail	—	50 µL
	Phosphatase Inhibitor Cocktail 2	—	50 µL
	Total		5 mL
2% SDS Base Buffer	10% SDS	2%	10 mL
	1 M Tris pH 7.4	50 mM	2.5 mL
	Milli-Q H_2O	—	37.5 mL
	Total		50 mL
SDS Extraction Buffer	2% SDS Base Buffer	—	4.9 mL
	Protease Inhibitor Cocktail	—	50 µL
	Phosphatase Inhibitor Cocktail 2	—	50 µL
	Total		5 mL
10X Tris-Glycine Buffer	Tris-Base	25 mM	30.3 g
	Glycine	192mM	144.1 g
	Milli-Q H_2O	—	1 L

Running Buffer	10X Tris-Glycine Buffer	1X	100 mL
	20% SDS	0.1% (w/v)	5 mL
	Milli-Q H_2O	—	895 mL
	Total		1 L
Transfer Buffer	10X Tris-Glycine Buffer	1X	100 mL
	Methanol	20% (v/v)	200 mL
	Milli-Q H_2O	—	700 mL
	Total		1 L

Acknowledgements

Completing this Dr. med. degree has been a long and challenging journey, and I would not have reached this point without the support of many people.

First, I would like to sincerely thank my supervisor, Prof. Thomas Köglsperger, for your consistent guidance, encouragement, and patience. The PhD growth curve you once drew reminded me that progress is rarely linear, and your support helped me stay on track through the more difficult phases of this work. I am also grateful to all colleagues in AG Köglsperger —our time together was not always smooth, but the experiences, both positive and challenging, have helped me grow in many ways.

I would like to thank Prof. Jochen Herms and the DZNE for providing the research platform and infrastructure that made this work possible. My thanks go to members of the Herms Lab for invaluable support, both scientific and personal. I am equally thankful to colleagues across DZNE departments and teams whose generous assistance and collaboration, whether large or small, supported this work in many ways.

My appreciation extends to Prof. Günter Höglinger for steady and unobtrusive support that gave me confidence and room to pursue this project. I am also grateful to the reviewers for their thoughtful evaluation and constructive feedback, which is substantial.

I thank our parents for unwavering support and trust, which gave me the freedom to study abroad without hesitation. Their love and encouragement have been the emotional foundation behind everything I do. I also gratefully acknowledge the China Scholarship Council (CSC) for financial support.

Finally, while the outcome of this journey may not fully match my early expectations, the experience has brought personal and professional growth far beyond any single result. This graduation is not an end but the beginning of a new chapter, with greater clarity, resilience, and hope for what lies ahead.

List of Publications

1. Hornung S, Vogl DP, Naltsas D, Volta BD, Ballmann M, Marcon B, Syed MMK, **Wu Y**, Spanopoulou A, Feederle R, Heidrich L, Bernhagen J, Koeglsperger T, Höglinger GU, Rammes G, Lashuel HA, Kapurniotu A. Multi-Targeting Macrocyclic Peptides as Nanomolar Inhibitors of Self- and Cross-Seeded Amyloid Self-Assembly of α-Synuclein. Angew Chem Int Ed Engl. 2025 Apr 1;64(14):e202422834. doi: 10.1002/anie.202422834. Epub 2025 Jan 31. PMID: 39822034.

2. **Wu Y**, Chen W, Gao P, Koeglsperger T. Insulin-Degrading Enzyme (IDE) Regulates the Balance Between Soluble and Insoluble Alpha-Synuclein. Parkinsonism Relat Disord. 2025 May 1. doi:10.1016/j.parkreldis.2025.107359.

Affidavit

Wu, Yiyang

Surname, first name

I hereby declare, that the submitted thesis entitled:

The Role of Insulin-Degrading Enzyme in Regulating α-Synuclein Aggregation and Toxicity.

is my own work. I have only used the sources indicated and have not made unauthorised use of services of a third party. Where the work of others has been quoted or reproduced, the source is always given.

I further declare that the dissertation presented here has not been submitted in the same or similar form to any other institution for the purpose of obtaining an academic degree.

Shanghai, 02.03.2026

Place, Date

Wu, Yiyang

Signature doctoral candidate

LMU LUDWIG-MAXIMILIANS-UNIVERSITÄT MÜNCHEN

Dekanat Medizinische Fakultät
Promotionsbüro

Confirmation of congruency between printed and electronic version of the doctoral thesis

Wu, Yiyang

Surname, first name

I hereby declare that the electronic version of the submitted thesis, entitled:

The Role of Insulin-Degrading Enzyme in Regulating α-Synuclein Aggregation and Toxicity.

is congruent with the printed version both in content and format.

Shanghai, 02.03.2026

Place, Date

Wu, Yiyang

Signature doctoral candidate